ornl

ORNL/TM-12276

OAK RIDGE NATIONAL LABORATORY

MARTIN MARIETTA

Measurements for the JASPER Program Axial Shield Re-measurement Experiment

F. J. Muckenthaler
R. R. Spencer
H. T. Hunter
J. L. Hull
A. Shono

MANAGED BY
MARTIN MARIETTA ENERGY SYSTEMS, INC.
FOR THE UNITED STATES
DEPARTMENT OF ENERGY

ORNL/TM-12276
Distribution Category
UC-534

Engineering Physics and Mathematics Division

MEASUREMENTS FOR THE JASPER PROGRAM AXIAL SHIELD RE-MEASUREMENT EXPERIMENT

F. J. Muckenthaler
R. R. Spencer
H. T. Hunter
J. L. Hull*
A. Shono**

Date Published: March 1993

Oak Ridge National Laboratory
Oak Ridge, Tennessee 37831-6363

Prepared for the
U.S. DOE Office of
Liquid Metal Converter Reactor

*Research Reactors Division
**Japan Power Reactor and Nuclear Fuel Development Corporation

Prepared by the
OAK RIDGE NATIONAL LABORATORY
Oak Ridge, Tennessee 37831
managed by
MARTIN MARIETTA ENERGY SYSTEMS, INC.
for the
U.S. Department of Energy
under contract DE-AC05-84OR21400

TABLE OF CONTENTS

LIST OF TABLES

LIST OF FIGURES

ABSTRACT

With one modification, this series of measurements is a repeat of several of the mockups that were investigated during the Axial Shield Experiment performed earlier for the Japanese-American Shielding Program for Experimental Research (JASPER) program at the Tower Shielding Facility (TSF). For these re-runs, slabs of lithiated paraffin, 10.16 cm thick and 152.4 cm on an edge, were placed between the spectrum modifier and the axial shield and directly behind the axial shield. Each of the slabs contained a void area that corresponded in dimension and location to the surface area of the seven hexagons in the axial shield plus the boron carbide (B_4C) collar that surrounded them. The lithiated paraffin was made part of the mockup to reduce the neutron contributions to the detector from those neutrons passing through the concrete surrounding the hexagon assemblies. The slabs were present in all of the mockups except one, for which the lithiated paraffin following the axial shield was removed.

Spectral and integral flux measurements were made behind the axial shield for six B_4C homogeneous-type assembly containing: (1) the B_4C rod bundle assembly; (2) the B_4C central blockage type; (4) the B_4C central sodium type; and (4) another B_4C homogeneous-type assembly. The neutron source was the Tower Shielding Reactor II (TSR-II) modified to give a flux typical of that incident on the axial shielding in a Liquid Metal Reactor (LMR).

1. INTRODUCTION

The Axial Shield Experiment, completed in 1991, was designed to extend the studies of the effectiveness of different axial shield designs located beyond the fission gas plenum and at the same time provide a comparison of the neutron attenuation characteristics of stainless steel and B_4C as they would be integrated into the design. The experiment served to provide data for verification of the analytical tools used in calculating the neutron streaming in each design. The results of the measurements, however, were in poor agreement with the calculated values obtained by the Japanese. The ratio of these values, calculated compared to measured, were much higher than the desired value of one.

It was assumed by the Japanese that this discrepancy was due to an incorrect determination of the water content in the axial shield concrete. Further attempts to determine the water content were not considered since such an analysis is very difficult. To minimize the contribution from the concrete, it was suggested that lithiated paraffin bricks in the form of a slab be placed on each face of the axial shield. The slabs would be 10.16 cm thick and 152.4 cm on an edge, with a void over the area occupied by the seven hexagons and the B_4C border surrounding the assemblies.

The same spectrum modifier preceded the axial shield as was used in the original axial shield measurements. Mockups were limited, however, to just those in the original measurements that contained the six B_4C homogeneous assemblies surrounding a central assembly whose composition also contained B_4C as the shield material to be studied. Measurements were made behind each mockup according to the program plan in Appendix A.

2. INSTRUMENTATION

The Bonner ball detection system used at the TSF consists of a series of different-sized polyethylene balls, each of which measures an integral of the neutron flux weighted by the energy-dependent response function for that ball. The detection device inside the ball consisted of a 5.1-cm-diam spherical proportional counter filled with boron trifluoride (BF_3) gas ($^{10}B/B$ concentration = 0.96) to a pressure of 0.5 atmospheres. In order to cover a range of neutron energies, the counter was used bare, covered with cadmium, or enclosed in various thicknesses of polyethylene shells surrounded by cadmium, each detector being identified by the diameter of the polyethylene sphere. Data from the Bonner ball measurements are predicted analytically by folding a calculated neutron spectrum with the Bonner ball response functions determined by Maerker et al.[1] and C. E. Burgart et al.[2]

An NE 213 liquid scintillator spectrometer system measured the neutron spectrum from about 800 keV to 15 MeV. This system makes use of pulse-shape discrimination to distinguish neutron pulses from gamma ray pulses. The resulting neutron pulse-height data obtained with the spectrometer were unfolded with the FERD code[3] to yield absolute neutron energy spectra.

Spherical proton-recoil counters, filled with hydrogen to pressures of 1, 3, and 10 atmospheres, covered the neutron energy range from about 50 keV to 1 MeV. Pulse-height data from the counters were unfolded with the SPEC-4 code,[4] which makes use of the unfolded NE 213 spectrum to correct for the contribution from higher-energy neutrons.

The Hornyak button detector consisted of a 0.635-cm-diam, 0.159-cm-thick button of lucite interspersed with zinc sulfide mounted on a photomultiplier tube. The calibration procedure was based on first exposing the scintillator to a 2 R/h gamma-ray dose rate and adjusting the amplifier gain so that a prescribed count rate was obtained at a pulse height setting (PHS) of 0.06 volts. This procedure kept the gain of the system constant on a daily basis. The button was then exposed to a known strength Californium (^{252}Cf) neutron source and a dose rate/count rate ratio obtained. However, for this particular experiment, it was necessary to obtain this neutron dose rate ratio at a higher PHS, namely 3.5 volts, to guard against a gamma ray contribution to the count rate when run in gamma ray fields greater than 2 R/h. Thus, even though the detector response no

longer corresponds to that of a dosimeter, it was elected to continue expressing the measurements in terms of a dose rate. At that PHS, even though the lower limit of the neutron energy response for the button is not known it did not detract from its usage to define the neutron streaming effect where small gaps existed in the mockup structure.

The measurements for each detector were referenced to the reactor power (watts) using the data from two fission chambers positioned along the reactor centerline as a basis. The response of these chambers as a function of reactor power level was established previously through several calorimetric measurements of the heat generated in the reactor during a temperature equilibrium condition (heat power run).

3. EXPERIMENTAL CONFIGURATION

The experimental program plan (see Appendix A) consists of repeat runs for several of the hexagonal mockups that were run previously in the Axial Shield Experiment, but this time a slab of lithiated paraffin was placed before the axial shield and another one following it. The slabs, 10.16 cm thick and 152.4 cm on an edge, were built from lithiated paraffin bricks. Each of the slabs contained a void whose shape closely mocked up the face of the axial shield corresponding to that area occupied by the seven hexagonal inserts and the B_4C border surrounding them. These slabs were included to enhance the neutron flux entering and then emerging from the hexagonal area with respect to those entering and leaving the concrete surrounding the B_4C collar. The hexagonal mockups represented LMR shield designs currently under study for the area directly above the reactor core and the fission gas plenum region. The only hexagons studied were those containing B_4C located in the center of six surrounding homogeneous B_4C hexagons. They were: (1) a central blockage in which the coolant flows around a central cylinder of B_4C; (2) a B_4C rod bundle in which the coolant flows around them; (3) a reverse of (1) in which the coolant flows through the center of the B_4C blockage; and (4) a homogeneous B_4C hexagon.

The neutron source was the TSR-II, whose emergent spectrum was modified to be similar to that predicted for the LMR design. It should be noted that the material thicknesses mentioned in the program plan are nominal, the actual thicknesses used are given in the left corner of the slabs shown in the various figures displayed in Appendix C.

3.1 SPECTRUM MODIFIER

The preanalysis calculation indicated that nominally 10 cm of iron, 10 cm of aluminum, 2.5 cm of boral, and 20.3 cm of "radial blanket" placed in that order in the TSR-II beam would provide a spectrum of neutrons representative of those incident on the axial shield from the LMR core. In the experiment (see Fig. 1) the iron component consisted of two rectangular slabs 5.20 and 5.13 cm thick, both 152.4 cm on an edge. The three aluminum slabs totalled 9.12 cm in thickness, and the boral was 2.54 cm thick, all having the same edge length as the iron slabs. Composition of the iron, aluminum, and boral are given in Tables 1, 2, and 3 respectively. (Note: All tables are included

in Appendix B.)

The uranium (UO_2) slabs used to represent the "radial blanket" were fabricated for earlier experiments performed in the Liquid Metal Fast Breeder Reactor (LMFBR) Program. They contained natural UO_2 pellets, 1.397-cm outside diameter (OD), enclosed in 1.524-cm OD aluminum cylinders. Between the aluminum and the pellets was a 0.00508- to 0.01016-cm annulus filled with argon. The cylinders were stacked side-by-side vertically having a triangular pitch of 1.608 cm. The space between the aluminum cylinders was filled with sodium. This arrangement of the rods and sodium was enclosed in an iron vessel having an overall thickness of 11.05 cm and a length of 152.4 cm on each side.

Each of the two radial blanket slabs used in this modifier contained 522 rods of natural UO_2 amounting to 64.6% of the volume of the slab. The rods were divided into seven rows, with alternating rows of 74 and 75 rods. The UO^2 density was 10.28 g/cc (94% of theoretical). The volume fraction of the aluminum cladding was 11.2% while that for the sodium and argon are 23.3% and about 1% respectively. The pellet stack length in each of the rods was approximately 121.9 cm. These rods were built by Numes Corporation in 1962 to conform, in general, to the then AEC/RDT designs for the Fast Flux Test Facility (FFTF). A schematic of the slab is shown in Fig. 2, with analyses of the UO_2 and aluminum given in Tables 4 and 5.

This spectrum modifier (SM-1) was surrounded by 20.3 cm (8 inches) of lithiated paraffin followed by up to 152.4 cm (60 inches) of concrete to minimize the neutrons scattering back into the slabs and to reduce the amount of background radiation reaching the detectors. The lithiated paraffin was shaped as small bricks 10.16 cm on an edge and 20.3 cm long (4-in-facing and 8-in-long) and the concrete consisted of blocks 61 cm on each edge and 30.48 cm thick. The composition of the lithiated paraffin and the concrete blocks have been presented in Tables 6 and 7 respectively.

3.2 BORON CARBIDE HOMOGENEOUS HEXAGON ASSEMBLY

The B_4C homogeneous assembly was composed of alternating pieces of B_4C and stainless steel, a schematic of which is shown in Fig. 3. The B_4C was contained in an aluminum vessel, the internal depth of the B_4C powder being 7.77 cm. The width of the B_4C was 14.73 cm from inside flat surface to inside flat surface with a wall thickness of

0.627 cm, making the outside dimensions of the container 15.98 cm. Each end plate thickness covering the B_4C was 1.123 cm. The density of the B_4C powder (120 grit) was 1.41 g/cc. An analysis of the B_4C powder is given in Table 8. Analysis of the 6061 aluminum was given earlier in Table 2. When the hexagon was placed in the configuration an aluminum-enclosed B_4C-loaded container was placed nearest the reactor, followed by alternating pieces of stainless steel and aluminum clad B_4C.

3.3 BORON CARBIDE ROD BUNDLE

The single assembly had a series of 37 rods of B_4C contained in stainless steel tubes equally spaced on a pitch of 2.38 cm throughout the aluminum assembly. The OD of the tubing was 2.06 cm, its inside diameter (ID) 1.897 cm, with each tube having a wall thickness of 0.0813 cm. The cap thickness on each end of the tube was 0.159 cm. The length of the B_4C inside each tube was 44.7 cm, giving a volume of 126.28 cc. The average density of the B_4C in the 37 rods was 1.30 g/cc. The average width of the aluminum was approximately 15.00 cm (flat surface to flat surface), and was surrounded, in this case, by nearly 0.465 cm of stainless steel as seen in Fig. 4. An analysis of the stainless steel tubes is given in Table 9.

3.4 BORON CARBIDE CENTRAL SODIUM CHANNEL ASSEMBLY

This particular hexagon mocks up the B_4C axial shield design with sodium flowing through the center of the assembly. A stainless steel can with 0.452-cm-thick walls served as the container for the B_4C as shown in Fig. 5. The length of the central aluminum cylinder was only 43.412 cm, with the two aluminum end pieces (0.794 cm thick) that enclose the B_4C providing the remainder of the 45 cm length. The 5760.1 cm volume of the B_4C in the assembly had a density of 1.39 g/cc.

3.5 BORON CARBIDE CENTRAL BLOCKAGE

In this assembly the central neutron shield was represented by a 12.98-cm-diam cylinder of B_4C surrounded by aluminum enclosed in a stainless steel blanket 0.462 cm thick (see Fig. 6). The length of the B_4C was limited to 44.05 cm so that each opening of the central cylinder could be covered with a 0.476-cm-thick aluminum plate. The volume of the B_4C was 5846.9 cc, having a density of 1.38 g/cc.

3.6 LEAD SLAB

A lead slab, 3.81 cm thick, was used to attenuate the gamma ray flux during the spectral measurements. The composition of the lead is given in Table 10.

3.7 SUPPORT STRUCTURE FOR THE ASSEMBLY MOCKUPS

The shield mockup was composed of a combination of seven subassemblies placed so that the axis of the central assembly coincided with the horizontal centerline of the reactor beam as it passed through the mockups. To support these assemblies in that fashion, a 45-cm-thick aluminum honeycomb structure, shown in Fig. 7, was secured in a modified concrete slab that had been used in an experiment prior to JASPER. The honeycomb itself represented a vertical path for sodium flow between assemblies in a typical LMR design. Between the aluminum honeycomb and the surrounding concrete slab was a layer of B_4C whose width varied as shown in Fig. 8. This B_4C had an average density of 1.33 g/cc. Between the B_4C and the concrete was a 0.952-cm iron envelope. The B_4C was covered on both ends of the honeycomb with a 0.81-cm-thick aluminum plate, making the total length of shield in that region about 46.6 cm (the mesh was only 45 cm long). The concrete slab was 304.8 cm wide, 213.4 cm high, and 45 cm thick. The analysis of the concrete in the slab is contained in Table 11. A picture of a typical experimental arrangement is shown in Fig. 9.

3.8 LITHIATED PARAFFIN SLAB SHIELD

A lithiated paraffin brick slab, 10.16 cm thick, was placed between the "radial blanket" and the axial shield mockup to enhance the neutron flux penetrating the hexagons with respect to the flux penetrating the concrete around the hexagons. A second slab of lithiated paraffin was placed behind the axial shield, again to inhibit neutrons reaching the detector from the concrete with respect to the hexagonal area. The slabs, 152.4 cm on an edge, contained a void at the center in the form of a cross whose dimensions closely matched the perimeter of the B_4C collar surrounding the seven hexagon assemblies in the axial shield. The shape and dimensions of the void are given in Fig. 10. A schematic of the lithiated paraffin slab superimposed on the seven hexagon arrangement is shown in Fig. 11.

3.9 AXIAL SHIELD

The mockup for the Axial Shield Experiment re-runs was the same as used in the Axial Shield Experiment in 1990. The shield to be examined was a combination of seven hexagonal subassemblies briefly described as a central hexagon surrounded by six others. For this series of measurements the outer six assemblies were always of the homogeneous B_4C type while the central hexagon varied as indicated in the program plan. The physical features of the hexagons were described earlier in this report. The spectrum modifier-axial shield combination provides a good representation of some of the U.S. ALMR shield designs and the loop-type (NIS) arrangement for the Japanese. The water content of the concrete in this slab was found to be 8.0 ± 0.5 wt percent[6] in an experiment conducted at the TSF.

3.10 BACKGROUND SHIELD

It has been the custom in the past to obtain background measurements as well as foreground measurements when the detectors were located at sufficient distance behind the mockups where neutron contributions to the detector from areas other than the mockup itself might not be negligible. For the background measurements a container of lithiated paraffin bricks, 91.4 x 91.4 cm on edge and 40.6 cm thick, would be placed between the detector and mockup in such a manner that contributions directly to the detector from the face of the last slab in the mockup would be substantially attenuated. The same approach was used for background measurements in this series of mockups, using the face of the lithiated paraffin slab that followed the axial shield as the enclosed area to be shadow-shielded from the detector. Upon removal of that lithiated paraffin slab to do Item IIB, the area of the axial shield previously covered by the lithiated paraffin slab was still assumed to be the area to be shadow-shielded.

A second set of background measurements was made for the mockups in Items IIA, IIB, and IIIA. In the initial axial shield measurements (1990-91), the program plan called for the background measurements to be made with only the area of the hexagons and B_4C surrounding them shadow-shielded. This type of background measurement was repeated in this experiment only behind the mockups in Items II, with and without the lithiated paraffin slab following the axial shield, and in Item IIIA. Though these three

measurements were not part of this experiment's original program plan, they were included in an attempt to provide data from which, when compared to the initial experimental data, it might be possible to determine the effectiveness of the lithiated paraffin slabs preceding and following the axial shield.

A schematic of the background shield used in this manner is shown in Fig. 12, where it is superimposed upon the area of the hexagons. To the left in the figure is a side view of the shield thickness, the width of the five bricks being equivalent to 50.8 cm. The bricks were placed directly behind the lithiated paraffin slab and remained there, unmoved, after the lithiated paraffin slab was removed for Item IIB.

4. MEASUREMENTS

The experimental program plan for this series of measurement re-runs limited the number of mockups to be studied, due to the run time available, to mockups containing boron carbide in the assemblies. The spectrum modifier was to remain the same as in the original measurements,[5] but it was to be followed by a slab of lithiated paraffin as discussed earlier in this report. The variables in the different mockups were the central assemblies which represented different approaches to physical combinations of the B_4C shielding material and the sodium coolant. The program plan does not include any mockups where the B_4C is replaced by stainless steel as in the original experiment.

The lithiated paraffin slab that followed the axial shield was identical to the one preceding it, both contained a void discussed earlier. This slab was removed for the measurements in Item IIB. It was necessary to insert a lead slab between the mockups and spectrometer in Items II and III to attenuate the gamma rays and provide a reasonable medium in which to obtain a neutron spectrum with good statistics in a reasonable time period.

It should be noted that even though there were changes in the order in which the measurements were made, the results have been reported in the order suggested by the program plan in Appendix A. Throughout this report, the words configuration, item, and mockup are used interchangeably when referring to the content of the program plan. At no time during these re-runs is the lithiated paraffin slab, before or after the axial shield, used as a point of reference for the detector measurements. For the spectrum modifier measurements, the reference is the radial blanket. Behind the axial shield the reference is the face of the hexagonal assembly.

4.1 SPECTRUM MODIFIER

Measurements behind the spectrum modifier and lithiated paraffin slab were limited to centerline measurements and radial traverses with the Bonner balls. Data was obtained on centerline with the 3-, 4-, 5-, 8-, 10-, and 12-inch Bonner balls at 30 and 150 cm behind the radial blanket. These results are listed in Tables 12 and 13 respectively. Mappings of the traverse flux distribution from south (S on the data tables) to north (N on the data tables) at 30 cm behind the radial blanket were made with the 3-,

5-, and 8-inch Bonner balls along the horizontal midplane. These results are listed in Tables 14, 15, and 16, and plotted in Figures 13, 14, and 15 respectively. A schematic of this mockup is contained in Fig. 1.

4.2 BORON CARBIDE HOMOGENEOUS SHIELD MOCKUP (ITEMS IIA, IIB)

This mockup behind the spectrum modifier and lithiated paraffin slab consisted of seven B_4C homogeneous assemblies placed in the aluminum mesh structure contained in the large concrete slab. This slab was placed directly behind the lithiated paraffin slab and centered on the reactor beam centerline. A second lithiated paraffin slab, identical in shape to the first one, was then placed directly behind the concrete slab to complete the mockup for Item IIA.

A slab of lead was placed behind the mockup for the neutron spectral measurements as shown in the schematic in Fig. 1. Measurements were made at 25 cm behind the lead and the spectrum from the NE 213 scintillator is given in Table 17 and plotted in Figure 16. The spectrum for the low-energy neutrons obtained with the hydrogen counter are given in Table 18 and plotted in Fig. 17. The 3-, 5-, and 10-inch Bonner ball results at this same location are given in Table 19. With the lead removed, both the horizontal traverses at 30 cm and the centerline measurements at 30 and 150 cm were made with the Bonner balls. The centerline measurements at 30 cm are given in Table 12, and the results at 150 cm are contained in Table 13. The horizontal traverse results are given in Tables 14, 15, and 16, and plotted in Figs. 13, 14, and 15. Results from the Hornyak button traverse at 2.4 cm behind the axial shield are listed in Table 20 and plotted in Fig. 18.

The scheduled background measurements called for in the data plan and reported in Table 13 were made using the shadow shield that was 91.4 cm x 91.4 cm x 40.6 cm thick. The added background measurements were made using the cross-shaped arrangement of lithiated paraffin bricks described earlier in this report (see Section 3.10). This shield was placed against the lithiated paraffin slab, thus covering the void within the slab. Results from these measurements are also included in Table 13 indicated by the notation "en".

The lithiated paraffin slab behind the axial shield (one closest to the detector) was then removed from the mockup without moving the shadow shield as positioned in Item

IIA. The background measurements were repeated and these results for Item IIB are also included in Table 13. The cross-shaped background shield was then removed and the scheduled measurements for Item IIB were initiated.

A lead slab was placed in the mockup to do the spectral measurement for Item IIB as shown in Fig. 19. The spectrometers were again located at 25 cm behind the lead on centerline. Results using the NE 213 detector are given in Table 21 and plotted in Fig. 20. Spectra obtained with the hydrogen-filled counters are listed in Table 22 and plotted in Fig. 21. Results from the 3-, 5-, and 10-inch Bonner ball measurements at this same location are given in Table 19. The lead slab was removed and traverses made at 30 cm behind the axial shield with the 3-, 5-, and 8-inch Bonner balls and the data are listed in Tables 14, 15, and 16, and plotted in Figures 13, 14, and 15. Centerline data at 30 and 150 cm are given in Tables 12 and 13. Results from the Hornyak button traverse at 2.4 cm behind the axial shield are listed in Table 20 and plotted in Fig. 18. The backgrounds this time were obtained using the 91.4 cm x 91.4 cm x 40.6 cm shadow shield. All of these measurements under Item IIB were obtained after completion of the program plan for Items IA, IIA, IIIA, IVA, and VA.

4.3 BORON CARBIDE ROD BUNDLE ASSEMBLY (ITEM IIIA)

For this mockup the B_4C rod bundle hexagon was surrounded by the six B_4C homogeneous assemblies to form the axial shield which was then followed by the lithiated paraffin slab used in Item IIA. Again spectral measurements were made with the NE 213 scintillator at 25 cm behind the lead slab that was added to the mockup as shown in Fig. 1. These results are listed in Table 23 and plotted in Fig. 22. The hydrogen counter results at the same location are given in Table 24 and plotted in Fig. 23. Bonner ball data at this same time location are given in Table 19.

The radial traverse results with the three Bonner balls at 30 cm beyond the Axial shield are given in Tables 14, 15, and 16, and plotted in Figs. 13, 14, and 15. The data from the Hornyak button traverse at 2.4 cm are in Table 20 and plotted in Fig. 18. The Bonner ball data on centerline at 30 and 150 cm behind the axial shield are in Tables 12 and 13.

4.4 BORON CARBIDE CENTRAL BLOCKAGE ASSEMBLY (ITEM IVA)

The central assembly in the previous mockup was replaced with the B_4C central-blockage-type assembly. The new axial shield mockup was followed by the same lithiated paraffin slab used in the previous mockup. Spectra were not obtained for this mockup, just the integral flux measurements were requested. Bonner balls were located on centerline at 30 and 150 cm behind the axial shield and these results are part of Tables 12 and 13. Traverses were made with the 3-, 5-, and 8-inch Bonner balls at 30 cm and these data are recorded in Tables 14, 15, and 16, and plotted in Figs. 13, 14, and 15. Hornyak button data at 2.4 cm behind the axial shield are part of Table 20 and plotted in Fig. 18.

4.5 BORON CARBIDE CENTRAL SODIUM CHANNEL ASSEMBLY (ITEM VA)

The mockup for Item VA was obtained by replacing the central blockage assembly with the central sodium channel assembly, keeping the same six B_4C homogeneous assemblies used in the previous mockups to surround it (see Fig. 1 for schematic details). Again spectral measurements were not requested. The Bonner ball results at 30 and 150 cm on centerline are given in Tables 12 and 13. The radial traverses with the 3-, 5-, and 8-inch Bonner balls generated data that are given in Tables 14, 15, and 16, and plotted in Figs. 13, 14, and 15. The Hornyak button data from the traverse at 2.4 cm are given in Table 20 and plotted in Fig. 18.

5. ANALYSIS OF EXPERIMENTAL ERRORS

The errors associated with the measurements are due to a number of uncertainties: (1) the sizes of the gaps between slabs, unavoidably introduced in the configurations; (2) in the positions of the detectors; (3) the detector count rate statistics and calibrations; (4) the reactor power determinations; and (5) the effects of the exposure of the configurations to the weather. Of these, the uncertainty due to the weather is the least understood and probably beyond simple estimation. The uncertainty lies in the amount of moisture between the slabs and in the lithiated paraffin surrounding them. During this experiment the mockups were covered with a plastic tarpaulin that would limit the amount of moisture reaching the slabs. Thus, for this experiment, the effect of the weather was assumed to be negligible.

Count rate statistics are expressed in a manner specific to each detector. For the NE 213 measurements, counting statistics and unfolding errors are included in the unfolding of the pulse-height spectra using the FERD code, with the resulting flux expressed in terms of lower and upper limits that represent a 68% confidence interval. Similar errors are expressed in the tabular data for the hydrogen measurements unfolded using SPEC4. Neither of the spectra, NE 213 or hydrogen counter, reflects the error in determining the reactor power since this error is not included in the unfolding program. This could be as much as ±5%.

The Bonner balls were calibrated on a daily basis using ^{252}Cf as a source, with the resulting count rates falling within about ±3% of an average value obtained throughout the years. Movement of the Bonner balls along a traversing mechanism can vary the detector location with respect to the configuration several millimeters on either side of a straight line. For the measurements perpendicular to the configuration centerline at 30 cm behind the configuration, such variations in the detector position could amount to a change in the count rate of about 2%. For the measurements on centerline beyond the 30 cm point, the error in positioning several millimeters either side of the selected location would lie within the statistics of the measurement.

The error in the Hornyak button measurements was largely dependent on the ability to maintain a constant temperature around the detector in the presence of large swings in the ambient temperature. Comparison of the calibration factors using a ^{252}Cf source made before and after a traverse showed an average spread of about 4%. This

variation, combined with error limits given for the power determinations, position locations, etc., does not project an overall error beyond that quoted for the other detectors, about ±5%.

The TSR-II power level for each measurement was determined from the output of two fission chambers located in the reactor shield along the midplane of the reactor. The response of these chambers to the reactor source was monitored prior to the experiment through the use of gold foils and this ratio, detector response to gold foil results, agreed within about 5% with a history of earlier such comparisons. These detectors were calibrated on a daily basis using a ^{252}Cf source, with the calibration values lying within about a 6% spread (±3% of an average value). During any one detector traverse in a given day, the variation in the reactor power indicated by the monitor outputs was at most only 3%; however, during the several months the experiment was being performed, the monitors indicated a spread in any one power level of about ±5%. Thus, the uncertainty in the reactor power determination was assumed to be ±5%.

Rather than calculate probable errors for each measurement in a series of measurements during a traverse, we prefer, in general, to quote a value for the error in the measurements for a given experiment. Thus, assuming the estimated upper limit for all the errors, the errors assigned to the Bonner ball and Hornyak button measurements should be less than ±10%.

ACKNOWLEDGEMENTS

The authors wish to express their appreciation to D. T. Ingersoll and J. V. Pace, III, of ORNL's Engineering Physics and Mathematics Division, to P. B. Hemmig of DOE/Washington, and to the JASPER working group from Japan for their participation and assistance in formulating the Experimental Program Plan. Gratitude is also expressed to the TSR-II operating crew of the Research Reactors Division and TSF assigned members of the Instrumentation and Controls Division for not only maintaining a viable source but for experimental help when needed. The authors are grateful to E. R. Specht, Rockwell International, W. H. Harless, General Electric Company, R. K. Disney, Westinghouse-ARD, W. L. Bunch, Westinghouse-Hanford for timely suggestions. Special thanks go to G. A. Marvin and S. A. Raby for their efforts in editing and preparing this report.

REFERENCES

1. R.E. Maerker et al., *Calibration of the Bonner Ball Neutron Detectors Used at the Tower Shielding Facility*, ORNL/TM-3465 (June 1971).

2. C. E. Burgart and M. B. Emmett, *Monte Carlo Calculations of the Response Functions of Bonner Ball Neutron Detectors*, ORNL/TM-3739 (April 1972).

3. B. W. Rust, D. T. Ingersoll, and W. R. Burrus, *A User's Manual for the FERDO and FERD Unfolding Codes*, ORNL/TM-8720 (September 1983).

4. J. O. Johnson and D. T. Ingersoll, *User's Guide for the Revised SPEC-4 Neutron Spectrum Unfolding Code*, ORNL/TM-7384 (August 1980).

5. F. J. Muckenthaler et al., *Measurements for the JASPER Program Axial Shield Experiment*, ORNL/TM-11829 (August 1991).

6. R. R. Spencer et al., *Measurement of Water Content of Concrete Shielding Used in JASPER Program*, ORNL/TM-12325 (to be published).

APPENDIX A

EXPERIMENTAL PROGRAM PLAN FOR THE JASPER AXIAL SHIELD RE-MEASUREMENT EXPERIMENT

I. Spectrum Modifier
   A. Spectrum Modifier (SM-1) (10 cm Fe + 9 cm Al + 2.5 cm boral + 20 cm Radial Blanket) + 10 cm lithiated paraffin with iris (see II)
      1. 3-, 4-, 5-, 8-, 10-, and 12-in Bonner ball measurements on centerline:
         a. 30 cm behind radial blanket
         b. 150 cm behind radial blanket (foreground and background)
      2. 3-, 5-, and 8-in Bonner ball horizontal traverses at 30 cm behind the radial blanket

II. Homogeneous Axial Shield Mockup
   A. SM-1 + 7 B_4C homogeneous-type assemblies (10 cm lithiated paraffin slab preceding and following axial shield)
      1. NE 213/hydrogen counter spectrum measurements on centerline as close as feasible behind the axial shield
      2. 3-, 5-, and 10-in Bonner ball on centerline at NE 213 location
      3. 3-, 4-, 5-, 8-, 10-, and 12-in Bonner ball measurements on centerline:
         a. 30 cm behind axial shield
         b. 150 cm behind axial shield (foreground and background)
      4. 3-, 5-, and 8-in Bonner ball horizontal traverses at 30 cm behind axial shield
      5. Hornyak button (0.25-in-diameter) horizontal traverse as close as feasible behind axial shield
   B. SM-1 + 7 B_4C homogeneous-type assemblies (10 cm lithiated paraffin slab preceding axial shield only)
      1. NE 213/hydrogen counter spectrum measurements on centerline as close as feasible behind the axial shield
      2. 3-, 5-, and 10-in Bonner ball on centerline at NE 213 location
      3. 3-, 4-, 5-, 8-, 10-, and 12-in Bonner ball measurements on centerline:
         a. 30 cm behind axial shield
         b. 150 cm behind axial shield (foreground and background)
      4. 3-, 5-, and 8-in Bonner ball horizontal traverses at 30 cm behind axial shield
      5. Hornyak button (0.25-in-diameter) horizontal traverse as close as feasible behind axial shield

III. Rod Bundle Axial Shield Mockup
- A. SM-1 + 6 B_4C homogeneous-type assemblies around one B_4C rod bundle hexagon assembly (10 cm lithiated paraffin slabs preceding and following axial shield)
  1. NE 213/hydrogen counter spectrum measurements on centerline as close as feasible behind axial shield
  2. 3-, 5-, and 10-in Bonner ball on centerline at NE 213 location
  3. 3-, 4-, 5-, 8-, 10-, and 12-in Bonner ball measurements on centerline:
     - a. 30 cm behind axial shield
     - b. 150 cm behind axial shield (foreground and background)
  4. 3-, 5-, and 8-in Bonner ball horizontal traverses at 30 cm behind axial shield
  5. Hornyak button (0.25-in-diameter) horizontal traverse as close as feasible behind axial shield

IV. Central Blockage Shield Mockup
- A. SM-1 + six B_4C homogeneous-type assemblies around one B_4C central blockage hexagon assembly (10 cm lithiated paraffin slabs preceding and following axial shield)
  1. 3-, 4-, 5-, 8-, 10-, and 12-in Bonner ball measurements on centerline:
     - a. 30 cm behind axial shield
     - b. 150 cm behind axial shield (foreground and background)
  2. 3-, 5-, and 8-in Bonner ball horizontal traverses at 30 cm behind axial shield
  3. Hornyak button (0.25-in-diam) horizontal traverse as close as feasible behind axial shield

V. Central Sodium Channel Shield Mockup (lithiated paraffin as in IIA)
- A. SM-1 + six B_4C homogeneous-type assemblies around one B_4C central sodium hexagon assembly (10 cm lithiated paraffin slab preceding and following axial shield)
  1. 3-, 4-, 5-, 8-, 10-, and 12-in Bonner ball measurements on centerline:
     - a. 30 cm behind axial shield
     - b. 150 cm behind axial shield (foreground and background)
  2. 3-, 5-, and 8-in Bonner ball horizontal traverses at 30 cm behind axial shield
  3. Hornyak button (0.25-in-diam) horizontal traverse as close as feasible behind axial shield

APPENDIX B

TABLES OF DATA

Table 1. Analysis of iron slabs (ρ = 7.86 g/cc) used in spectrum modifier

Element	wt %
Fe	98.4
C	.25
Cr	.15
Cu	.03
Mn	1.0
Mo	.02
Ni	.05
Si	.25

Table 2. Analysis of 6061 aluminum (ρ = 2.70 g/cc)

Element	wt %	ppm
Al	97.5	
Cr	.22	
Cu	.23	
Fe	.47	
Mg	.86	
Mn	.01	
Si	.63	
Ti	.042	
Zn	.07	
Li		3
Ni		50
Sn		<10
V		150

Table 3. Composition of boral slabs used in spectrum modifier

	(B_4C - 40-43 vol % in B_4C-Al mixture)		
Component	Density (g/cc)	Elemental Composition (wt %)	With Al Cladding (wt %)
B_4C	2.3		
Al	2.70	65	~75
B		27.5	~19.6
C		7.5	~5.4

Table 4. Composition of UO_2 radial blanket

Component	vol %	Density (g/cc)
UO_2 (pellets)	64.6	10.28
Al (8001)	11.2	2.8
Na	23.2	0.92
Void	1.0	----

U content 88.18 wt % of UO_2

Isotope %

^{234}U	.0053	^{236}U	---
^{235}U	.713	^{238}U	99.28

Metallic Impurities in UO_2 (ppm)*

Al	<20	Cu	1	Na	<20
B	<1	F	<2	Ni	<10
Be	<2	Fe	<20	Pb	<4
Bi	<2	H_2O	2.1	Si	<20
C	<10	Li	<1	Sn	<2
Ca	<20	Mg	<10	Ta	<25
Cd	<0.5	Mn	<4	Tu	<4
Cl	<3.3	Mo	<10	W	<25
Co	<2	N	54	Zr	<25
Cr	<10				

*ppm = parts per million

Table 5. Analysis of aluminum used in UO_2 radial blanket cladding (ρ = 2.7 g/cc)

Element	wt %	ppm
Al	Major	
Fe	.59	
Ni	1.13	
B		<6
Be		<20
Cd		<20
Co		<20
Cr		<6
Cu		52.9
Li		6
Mg		3.04
Mn		11.2
Mo		<6
Pb		<20
Si		27.5
Sn		<60
T		<2000
Ti		65.5
V		44.2
W		<60
Zr		<20

Table 6. Composition of lithiated-paraffin bricks (ρ = 1.15 g/cc)

Component	wt %
C_nH_{2n+2}	60
Li_2CO_3	40

Table 7. Analysis of 61-cm x 61-cm x 30.5-cm (ρ = 2.40 g/cc) concrete blocks used to surround configuration

Component	wt%	Component	wt%
CO_3	41.9	Al_2O_3	2.2
Ca	27.4	Fe_2O_3	.60
SiO_2	18.1	SO_3	.32
H_2O	4.0	P_2O_5	.035
Mg	3.66	K	.30
O_2	1.4		

The water content in these blocks was found to be 8.3 ± 0.5 wt percent.[6]

Table 8. Analysis of B_4C in hexagon assemblies (ρ = 1.41 g/cc)

Sample #	% Boron	% Carbon	% Boron Nitride
1	78.2	20.0	1.8
2	78.2	20.4	1.6
3	78.2	20.0	1.8
Element	**Sample #1***	**Sample #2***	**Sample #3***
Al	5	10	3
Ca	5	5	30
Co	<1	<1	<1
Cr	1	3	3
Cl	3	5	3
Cu	3	3	3
Fe	10	50	50
Mg	<5	10	5
Mn	1	3	5
Na	5	10	30
P	3	3	3
Sc	3	3	3
Si	<20	<20	<20
Ti	3	3	10

*Parts per million

Table 9. Analysis of 304 stainless steel in tubes used for boron carbide rod bundle (ρ = 7.92 g/cc)

Element	Wt%
Fe	70.3
Co	0.11
Cr	18.3
Cu	0.37
Mn	1.24
Mo	0.32
Ni	9.0
Si	.31
Ti	.023

Table 10. Analysis of lead slab used as part of mockup in IIA, IIB (ρ = 11.35 g/cc)

Element	wt%	PPM
Lead	99.9	
Al		<3
Ag		30
B		<1
Ca		1
Cr		10
Cu		800
Fe		1
Li		20
Mg		<3
Mn		5
Na		1
Ni		30
P		5
Si		<3
Sn		30

Table 11. Analysis of concrete in axial shield concrete slab (ρ = 2.40 g/cc)

Element	Axial shield concrete (%)
Free H_2O	0.97
Bound H_2O	2.44
LOI*	35.25
SiO_2	9.41
Fe_2O_3	0.94
Al_2O_3	1.57
CaO	36.96
MgO	13.2
Na_2O	0.022
K_2O	0.53
SO_3	0.16
P_2O_5	0.10
CO_3	43.9

*LOI (Lost on Ignition) includes the free and bound H_2O and SO_3. To obtain correct wt% for the materials, multiply CO_3 value by .7334 to get CO_2 and when summed the LOI values should not be included.

The water content in this shield was found to be 8.0 ± 0.5 wt percent.[6]

Table 12. Bonner ball measurements on centerline at 30 cm behind the mockups (Items IA, IIA, IIB, IIIA, IVA, VA)

Configuration[a]	Bonner ball count rates ($s^{-1}W^{-1}$)					
	3-inch-diam ball	4-inch-diam ball	5-inch-diam ball	8-inch-diam ball	10-inch-diam ball	12-inch-diam ball
IA	6.07 (2)[b]	1.89 (3)	2.53 (3)	1.85 (3)	9.02 (2)	4.56 (2)
IIA	5.56 (-1)	2.00 (0)	3.10 (0)	2.79 (0)	1.76 (0)	9.24 (-1)
IIB	5.50 (-1)	1.94 (0)	2.95 (0)	2.74 (0)	1.66 (0)	9.26 (-1)
IIIA	6.42 (-1)	2.31 (0)	3.50 (0)	2.98 (0)	1.79 (0)	9.84 (-1)
IVA	5.95 (-1)	2.12 (0)	3.20 (0)	2.88 (0)	1.70 (0)	9.39 (-1)
VA	8.46 (-1)	2.98 (0)	4.31 (0)	3.36 (0)	1.90 (0)	1.01 (0)

[a]See experimental program plan in Appendix A for description of configurations.
[b]Read: 6.07×10^2.

Table 13. Bonner ball measurements on centerline at 150 cm behind the mockup (Items IA, IIA, IIB, IIIA, IVA, VA)

	Bonner ball count rates ($s^{-1}W^{-1}$)					
	3-inch-diam ball		4-inch-diam ball		5-inch-diam ball	
Configuration[a]	Foreground[b]	Background[c]	Foreground	Background	Foreground	Background
IA	5.20 (1)[d]	5.05 (0)	1.52 (2)	9.61 (0)	2.06 (2)	1.05 (1)
IIA	7.28 (-2)	5.74 (-3)	2.42 (-1)	1.10 (-2)	3.58 (-1)	1.28 (-2)
IIB	1.05 (-1)	1.12 (-2)	3.08 (-1)	2.19 (-2)	4.33 (-1)	2.48 (-2)
IIIA	8.43 (-2)	6.81 (-3)	2.84 (-1)	1.28 (-2)	4.09 (-1)	1.42 (-2)
IVA	7.88 (-2)	6.51 (-3)	2.66 (-1)	1.23 (-2)	3.81 (-1)	1.40 (-2)
VA	1.04 (-1)	6.19 (-3)	3.39 (-1)	1.22 (-2)	4.79 (-1)	1.39 (-2)
IIA[e]		6.20 (-3)		1.25 (-2)		1.54 (-2)
IIB[e]		2.47 (-2)		4.88 (-2)		5.86 (-2)
IIIA[e]		6.54 (-3)		1.26 (-2)		1.55 (-2)

Table 13. (continued)

	Bonner ball count rates ($s^{-1}W^{-1}$)					
	8-inch-diam ball		10-inch-diam ball		12-inch-diam ball	
Configuration	Foreground	Background	Foreground	Background	Foreground	Background
IA	1.51 (2)	5.93 (0)	7.85 (1)	3.01 (0)	4.01 (1)	1.52 (0)
IIA	2.98 (-1)	7.39 (-3)	1.78 (-1)	4.02 (-3)	9.98 (-2)	2.22 (-3)
IIB	3.57 (-1)	1.48 (-2)	2.20 (-1)	8.40 (-3)	1.23 (-1)	4.59 (-3)
IIIA	3.24 (-1)	8.06 (-3)	1.86 (-1)	4.39 (-3)	1.06 (-1)	2.39 (-3)
IVA	3.11 (-1)	7.67 (-3)	1.79 (-1)	4.32 (-3)	1.04 (-1)	2.33 (-3)
VA	3.61 (-1)	7.76 (-3)	2.34 (-1)	4.39 (-3)	1.29 (-1)	2.40 (-3)
IIA		1.25 (-2)		8.37 (-3)		5.39 (-3)
IIB		4.42 (-2)		2.88 (-2)		1.77 (-2)
IIIA		1.17 (-2)		7.68 (-3)		4.98 (-3)

[a]See experimental program plan in Appendix A for description of configurations.
[b]Count rate without shadow shield between detector and configuration.
[c]Count rate with shadow shield between detector and configuration.
[d]Read: 5.20×10^{1}.
[e]Count rate with shadow shield shape that matched the shape of the seven hexagons (see schematic in Figure 12 for dimensions).

Table 14. 3-inch Bonner ball traverses through the horizontal midplane at 30 cm behind a series of configurations (Items IA, IIA, IIB, IIIA, IVA, VA)

Distance from centerline (cm)	Bonner ball count rates ($s^{-1}W^{-1}$)					
	Item IA[a]	Item IIA	Item IIB	Item IIIA	Item IVA	Item VA
100 S	2.29 (1)[b]	2.88 (-2)	6.59 (-2)		2.81 (-2)	2.82 (-2)
90	3.12 (1)	3.43 (-2)	8.78 (-2)	3.49 (-2)	3.43 (-2)	3.48 (-2)
80	4.70 (1)	3.97 (-2)	1.17 (-1)	4.16 (-2)	3.87 (-2)	4.04 (-2)
70	6.66 (1)	4.73 (-2)	1.55 (-1)	4.92 (-2)	4.77 (-2)	4.82 (-2)
60	9.40 (1)	6.62 (-2)	2.02 (-1)	7.01 (-2)	6.61 (-2)	6.82 (-2)
50	1.44 (2)	1.07 (-1)	2.60 (-1)	1.13 (-1)	1.07 (-1)	1.09 (-1)
40	2.37 (2)	1.76 (-1)	3.25 (-1)	1.89 (-1)	1.80 (-1)	1.87 (-1)
35	3.07 (2)	2.36 (-1)		2.46 (-1)	2.32 (-1)	2.39 (-1)
30	3.74 (2)	2.92 (-1)	3.98 (-1)	3.10 (-1)	2.95 (-1)	3.07 (-1)
25	4.45 (2)	3.58 (-1)		3.82 (-1)	3.60 (-1)	3.70 (-1)
20	5.09 (2)	4.10 (-1)	4.75 (-1)			4.33 (-1)
17		4.53 (-1)		4.79 (-1)	4.70 (-1)	4.82 (-1)
15		4.80 (-1)				5.16 (-1)
12		5.14 (-1)				5.68 (-1)
10	5.89 (2)	5.34 (-1)	5.61 (-1)			6.33 (-1)
9				5.75 (-1)	5.91 (-1)	
8		5.37 (-1)				7.07 (-1)
6					6.03 (-1)	
5		5.49 (-1)				7.88 (-1)
3					5.81 (-1)	
2.5						8.23 (-1)
0	6.17 (2)	5.51 (-1)	5.79 (-1)	6.22 (-1)	5.80 (-1)	8.32 (-1)
2.5						8.33 (-1)
3					5.85 (-1)	
5		5.48 (-1)				7.82 (-1)
6					6.09 (-1)	
8		5.55 (-1)				7.22 (-1)
9				5.94 (-1)	5.95 (-1)	
10	5.75 (2)	5.37 (-1)	5.68 (-1)			6.61 (-1)
12		5.20 (-1)				5.91 (-1)
15		4.78 (-1)				5.29 (-1)
17		4.65 (-1)		5.00 (-1)	4.69 (-1)	5.01 (-1)
20	4.91 (2)	4.14 (-1)	4.78 (-1)			4.55 (-1)
25	4.30 (2)	3.62 (-1)		3.94 (-1)	3.64 (-1)	3.92 (-1)
30	3.63 (2)	3.01 (-1)	4.11 (-1)	3.28 (-1)	3.04 (-1)	3.19 (-1)
35	2.84 (2)	2.38 (-1)		2.61 (-1)	2.41 (-1)	2.51 (-1)
40	2.24 (2)	1.84 (-1)	3.27 (-1)	2.04 (-1)	1.83 (-1)	1.97 (-1)
50	1.38 (2)	1.07 (-1)	2.61 (-1)	1.22 (-1)	1.12 (-1)	1.14 (-1)
60	8.69 (1)	6.97 (-2)	2.02 (-1)	7.49 (-2)	6.91 (-2)	7.10 (-2)
70	6.05 (1)	4.82 (-2)	1.50 (-1)	5.02 (-2)	4.67 (-2)	4.88 (-2)
80	4.13 (1)	3.95 (-2)	1.13 (-1)	4.06 (-2)	3.82 (-2)	4.08 (-2)
85	3.37 (1)				3.46 (-2)	
90						
100 N			6.66 (-2)			

[a]See experimental program plan in Appendix A for description of configurations.
[b]Read: 2.29×10^{1}.

Table 15. 5-inch Bonner ball traverses through the horizontal midplane at 30 cm behind a series of configurations (Items IA, IIA, IIB, IIIA, IVA, VA)

Distance from centerline (cm)	Bonner ball count rates ($s^{-1}W^{-1}$)					
	Item IA[a]	Item IIA	Item IIB	Item IIIA	Item IVA	Item VA
100 S	6.06 (1)[b]	8.40 (-2)	2.09 (-1)		8.68 (-2)	8.53 (-2)
90	8.58 (1)	1.07 (-1)	2.78 (-1)	1.07 (-1)	1.08 (-1)	1.08 (-1)
80	1.30 (2)	1.36 (-1)	3.87 (-1)	1.38 (-1)	1.40 (-1)	1.37 (-1)
70	1.97 (2)	1.84 (-1)	5.22 (-1)	1.91 (-1)	1.89 (-1)	1.89 (-1)
60	3.01 (2)	2.89 (-1)	7.23 (-1)	3.00 (-1)	2.96 (-1)	2.99 (-1)
50	4.98 (2)	5.05 (-1)	9.84 (-1)	5.29 (-1)	5.28 (-1)	5.31 (-1)
40	8.86 (2)	9.28 (-1)	1.35 (0)	9.62 (-1)	9.58 (-1)	9.57 (-1)
35	1.21 (3)	1.22 (0)		1.29 (0)	1.27 (0)	1.26 (0)
30	1.50 (3)	1.59 (0)	1.85 (0)	1.64 (0)	1.66 (0)	1.64 (0)
25	1.81 (3)			2.04 (0)	2.04 (0)	2.02 (0)
20	2.16 (3)	2.24 (0)	2.39 (0)		2.40 (0)	2.39 (0)
17				2.62 (0)	2.64 (0)	2.60 (0)
15					2.80 (0)	2.78 (0)
10	2.43 (3)	2.91 (0)	2.95 (0)		3.29 (0)	3.41 (0)
9				3.22 (0)		
8					3.34 (0)	3.65 (0)
5		3.02 (0)			3.35 (0)	3.96 (0)
0	2.59 (3)	3.03 (0)	3.05 (0)	3.46 (0)	3.34 (0)	4.19 (0)
5		3.01 (0)			3.39 (0)	3.95 (0)
8					3.33 (0)	3.66 (0)
9				3.36 (0)		
10	2.46 (3)	2.90 (0)	2.97 (0)		3.22 (0)	3.42 (0)
15					2.81 (0)	2.78 (0)
17				2.77 (0)	2.61 (0)	2.61 (0)
20	2.07 (3)	2.22 (0)	2.39 (0)		2.39 (0)	2.36 (0)
25	1.77 (3)			2.17 (0)	2.04 (0)	2.01 (0)
30	1.47 (3)	1.58 (0)	1.87 (0)	1.78 (0)	1.67 (0)	1.63 (0)
35	1.13 (3)			1.41 (0)	1.29 (0)	1.29 (0)
40	8.41 (2)	9.56 (-1)	1.35 (0)	1.08 (0)	9.91 (-1)	9.61 (-1)
50	4.83 (2)	5.20 (-1)	9.94 (-1)	5.96 (-1)	5.37 (-1)	5.17 (-1)
60	2.87 (2)	2.98 (-1)	7.28 (-1)	3.35 (-1)	3.06 (-1)	3.00 (-1)
70	1.79 (2)	1.81 (-1)	5.18 (-1)	2.02 (-1)	1.85 (-1)	1.85 (-1)
80	1.18 (2)	1.30 (-1)	3.78 (-1)	1.40 (-1)	1.33 (-1)	1.32 (-1)
85	9.36 (1)					
90			2.83 (-1)			
100 N			2.05 (-1)			

[a]See experimental program plan in Appendix A for description of configurations.
[b]Read: 6.06×10^{1}.

Table 16. 8-inch Bonner ball traverses through the horizontal midplane at 30 cm behind a series of configurations (Items IA, IIA, IIB, IIIA, IVA, VA)

Distance from centerline (cm)	Bonner ball count rates ($s^{-1}W^{-1}$)					
	Item IA[a]	Item IIA	Item IIB	Item IIIA	Item IVA	Item VA
100 S	3.53 (1)[b]	7.16 (-2)	1.75 (-1)		7.18 (-2)	7.23 (-2)
90	5.24 (1)	9.12 (-2)	2.38 (-1)	9.38 (-2)	8.99 (-2)	9.22 (-2)
80	8.14 (1)	1.16 (-1)	3.24 (-1)	1.19 (-1)	1.13 (-1)	1.15 (-1)
70	1.25 (2)	1.62 (-1)	4.45 (-1)	1.73 (-1)	1.57 (-1)	1.62 (-1)
60	2.00 (2)	2.60 (-1)	6.12 (-1)	2.79 (-1)	2.61 (-1)	2.64 (-1)
50	3.45 (2)	4.60 (-1)	8.49 (-1)	5.00 (-1)	4.56 (-1)	4.64 (-1)
40	6.14 (2)	8.28 (-1)	1.16 (0)	9.01 (-1)	8.27 (-1)	8.49 (-1)
35				1.21 (0)		1.14 (0)
30	1.04 (3)	1.42 (0)	1.60 (0)	1.52 (0)	1.42 (0)	1.45 (0)
25				1.88 (0)		1.80 (0)
20	1.47 (3)	2.05 (0)	2.10 (0)		2.08 (0)	2.13 (0)
17				2.40 (0)		
15						2.47 (0)
10	1.70 (3)	2.51 (0)	2.54 (0)		2.66 (0)	2.83 (0)
9				2.83 (0)		
5						3.11 (0)
0	1.80 (3)	2.70 (0)	2.70 (0)	3.03 (0)	2.88 (0)	3.25 (0)
5						3.10 (0)
9				2.83 (0)		
10	1.68 (3)	2.55 (0)	2.60 (0)		2.66 (0)	2.83 (0)
15						2.45 (0)
17				2.38 (0)		
20	1.40 (3)	2.04 (0)	2.18 (0)		2.11 (0)	2.09 (0)
25				1.87 (0)		1.76 (0)
30	9.78 (2)	1.41 (0)	1.68 (0)	1.53 (0)	1.44 (0)	1.45 (0)
35				1.19 (0)		1.14 (0)
40	5.75 (2)	8.44 (-1)	1.21 (0)	9.07 (-1)	8.90 (-1)	8.55 (-1)
50	3.07 (2)	4.80 (-1)	8.78 (-1)	5.00 (-1)	4.87 (-1)	4.69 (-1)
60	1.79 (2)	2.65 (-1)	6.33 (-1)	2.88 (-1)	2.70 (-1)	2.60 (-1)
70	1.10 (2)	1.61 (-1)	4.61 (-1)	1.79 (-1)	1.64 (-1)	1.57 (-1)
80	6.97 (1)	1.11 (-1)	3.34 (-1)	1.16 (-1)	1.13 (-1)	1.08 (-1)
85				1.03 (-1)		
90			2.46 (-1)			
100 N			1.79 (-1)			

[a]See experimental program plan in Appendix A for description of configurations.
[b]Read: 3.53×10^{1}.

Table 17. Spectrum of high-energy neutrons (>0.8 MeV) on centerline at 25 cm behind the lead slabs (Item IIA): Run 7940

Neutron Energy (MeV)	Flux (neutrons $cm^{-2}MeV^{-1}kW^{-1}s^{-1}$) Lower Limit	Upper Limit	Neutron Energy (MeV)	Flux (neutrons $cm^{-2}MeV^{-1}kW^{-1}s^{-1}$) Lower Limit	Upper Limit
8.11E -01	3.45E +02	3.49E +02	5.94E +00	9.61E +00	9.97E +00
9.07E -01	3.74E +02	3.77E +02	6.25E +00	8.16E +00	8.57E +00
1.01E +00	3.27E +02	3.29E +02	6.55E +00	7.12E +00	7.46E +00
1.11E +00	2.56E +02	2.57E +02	6.84E +00	6.33E +00	6.58E +00
1.20E +00	1.95E +02	1.97E +02	7.24E +00	5.37E +00	5.56E +00
1.31E +00	1.56E +02	1.57E +02	7.74E +00	4.12E +00	4.37E +00
1.41E +00	1.39E +02	1.41E +02	8.24E +00	3.11E +00	3.37E +00
1.51E +00	1.32E +02	1.33E +02	8.76E +00	2.37E +00	2.50E +00
1.61E +00	1.26E +02	1.27E +02	9.26E +00	1.79E +00	1.90E +00
1.71E +00	1.19E +02	1.20E +02	9.74E +00	1.37E +00	1.46E +00
1.81E +00	1.13E +02	1.14E +02	1.03E +01	1.02E +00	1.10E +00
1.93E +00	1.06E +02	1.07E +02	1.08E +01	7.48E -01	8.18E -01
2.10E +00	9.43E +01	9.54E +01	1.12E +01	5.51E -01	6.04E -01
2.30E +00	7.88E +01	7.98E +01	1.18E +01	3.71E -01	4.13E -01
2.50E +00	6.38E +01	6.46E +01	1.24E +01	2.24E -01	2.65E -01
2.70E +00	5.12E +01	5.20E +01	1.32E +01	1.32E -01	1.57E -01
2.90E +00	4.30E +01	4.38E +01	1.40E +01	6.67E -02	8.81E -02
3.10E +00	3.71E +01	3.80E +01	1.48E +01	4.07E -02	5.69E -02
3.30E +00	3.23E +01	3.30E +01	1.56E +01	2.24E -02	3.73E -02
3.50E +00	2.90E +01	2.99E +01	1.65E +01	6.23E -03	1.53E -02
3.71E +00	2.71E +01	2.77E +01	1.75E +01	-7.43E -04	5.36E -03
3.91E +00	2.55E +01	2.60E +02	1.85E +01	-2.49E -03	3.45E -03
4.15E +00	2.35E +01	2.40E +01	1.95E +01	-2.39E -03	1.84E -03
4.45E +00	2.04E +01	2.08E +01	2.05E +01	-3.70E -03	2.47E -03
4.75E +00	1.72E +01	1.76E +01	2.16E +01	-3.61E -03	2.87E -03
5.04E +00	1.47E +01	1.51E +01	2.26E +01	-2.05E -03	2.12E -03
5.34E +00	1.28E +01	1.31E +01	2.35E +01	-1.70E -03	1.99E -03
5.64E +00	1.12E +01	1.16E +01			

E1 (MeV)	E2 (MeV)	Integral neutrons $cm^{-2}kW^{-1}s^{-1}$	Error neutrons $cm^{-2}kW^{-1}s^{-1}$
0.811	1.000	6.86E +01	2.73E -01
1.000	1.200	5.25E +01	1.70E -01
1.200	1.600	5.91E +01	3.03E -01
1.600	2.000	4.56E +01	2.40E -01
2.000	3.000	6.66E +01	4.52E -01
3.000	4.000	3.06E +01	3.58E -01
4.000	6.000	3.23E +01	4.02E -01
6.000	8.000	1.24E +01	2.80E -01
8.000	10.000	4.47E +00	1.45E -01
10.000	12.000	1.42E +00	6.20E -02
12.000	16.000	4.44E -01	4.68E -02
16.000	20.000	1.50E -02	1.31E -02
3.000	10.000	7.97E +01	1.19E +00
1.500	15.000	2.07E +02	2.05E +00
3.000	12.000	8.12E +01	1.25E +00

Table 18. Neutron spectrum (50 keV to 1.4 MeV) on centerline at 25 cm behind the lead slab (Item IIA) Runs 1610.B, 1610.C, 1610.A

N	Energy Boundary (MeV)		Flux (neutrons $cm^{-2}MeV^{-1}kW^{-1}s^{-1}$)	Error (%)
		RUN 1610.B		
1	0.0397	0.0450	3.08E +03	3.37
2	0.0450	0.0538	2.75E +03	2.53
3	0.0538	0.0626	2.71E +03	2.89
4	0.0626	0.0750	2.68E +03	2.25
5	0.0750	0.0873	2.09E +03	3.24
6	0.0873	0.1032	1.32E +03	4.34
7	0.1032	0.1208	1.42E +03	4.09
8	0.1208	0.1420	1.57E +03	3.36
9	0.1420	0.1684	1.13E +03	4.00
10	0.1684	0.1984	9.49E +02	4.70
		RUN 1610.C		
1	0.1446	0.1715	1.09E +03	1.66
2	0.1715	0.1984	8.86E +02	2.36
3	0.1984	0.2320	8.22E +02	2.32
4	0.2320	0.2724	8.80E +02	2.04
5	0.2724	0.3195	8.28E +02	2.10
6	0.3195	0.3800	6.88E +02	2.18
7	0.3800	0.4473	5.21E +02	2.96
8	0.4473	0.5280	5.57E +02	2.57
9	0.5280	0.6154	5.57E +02	2.64
10	0.6154	0.7297	4.99E +02	2.30
		RUN 1610.A		
1	0.5243	0.6216	5.32E +02	1.68
2	0.6216	0.7297	4.70E +02	1.87
3	0.7297	0.8595	4.06E +02	1.92
4	0.8595	1.0108	3.43E +02	2.04
5	1.0108	1.1838	2.36E +02	2.69
6	1.1838	1.4000	1.43E +02	3.62

Table 19. Bonner ball measurements on centerline at NE 213 location (Items IIA, IIB, IIIA)

Configuration[a]	Detector Location	Bonner ball count rates ($s^{-1}W^{-1}$) 3-in-Diam Ball[c]	5-in-Diam Ball	10-in-Diam Ball
IIA	25 cm behind lead[b]	2.77 (-1)[d]	1.47 (0)	8.45 (-1)
IIB	25 cm behind lead	4.15 (-1)	2.16 (0)	1.20 (0)
IIIA	25 cm behind lead	3.12 (-1)	1.65 (0)	8.78 (-1)

[a]See experimental program plan in Appendix A for description of configurations.
[b]Lead slab between configuration and detector (see schematics).
[c]Foreground only. Count rates without shadow shield between detector and lead slab.
[d]Read: 2.77×10^{-1}.

Table 20. Hornyak button traverses through the horizontal midplane at 2.4 cm behind a series of configurations (Items IIA, IIB, IIIA, IVA, VA)

Distance from centerline (cm)	Bonner ball count rates ($s^{-1}W^{-1}$)				
	Item IIA[a]	Item IIB	Item IIIA	Item IVA	Item VA
70 S		1.42 (-4)			
60		2.21 (-4)			
50		3.20 (-4)			
40		4.45 (-4)			
35		5.07 (-4)			
30		6.50 (-4)			
28.5	8.12 (-4)[b]				
28.4					8.40 (-4)
28.3			7.85 (-4)		
28		7.44 (-4)		8.14 (-4)	
26		8.72 (-4)			
25	1.06 (-3)		1.03 (-3)	1.04 (-3)	1.11 (-3)
24		9.83 (-4)			
22		1.10 (-3)			
20	1.35 (-3)	1.21 (-3)	1.31 (-3)	1.31 (-3)	1.43 (-3)
16		1.40 (-3)			
15	1.62 (-3)		1.57 (-3)	1.61 (-3)	1.72 (-3)
12		1.60 (-3)			
10	1.82 (-3)		1.80 (-3)	1.85 (-3)	2.00 (-3)
8.3	1.94 (-3)	1.72 (-3)	1.89 (-3)	1.94 (-3)	2.10 (-3)
7.7			1.99 (-3)	2.01 (-3)	2.17 (-3)
7.0			1.97 (-3)	2.02 (-3)	2.21 (-3)
6.0			2.01 (-3)	2.06 (-3)	2.24 (-3)
5	1.98 (-3)				
4		1.77 (-3)	2.09 (-3)	2.14 (-3)	2.31 (-3)
2.5			2.08 (-3)	2.16 (-3)	2.34 (-3)
0	1.97 (-3)	1.78 (-3)	2.09 (-3)	2.19 (-3)	2.37 (-3)
2.5			2.10 (-3)	2.16 (-3)	2.36 (-3)
4		1.78 (-3)	2.06 (-3)	2.16 (-3)	2.31 (-3)
5	1.96 (-3)				
6			2.02 (-3)	2.10 (-3)	2.28 (-3)
7			1.99 (-3)	2.05 (-3)	2.26 (-3)
7.7			1.99 (-3)	2.02 (-3)	2.16 (-3)
8.3	1.91 (-3)	1.76 (-3)	1.93 (-3)	1.97 (-3)	2.14 (-3)
10	1.83 (-3)		1.82 (-3)	1.87 (-3)	2.05 (-3)
12		1.59 (-3)			
15	1.63 (-3)		1.59 (-3)	1.62 (-3)	1.77 (-3)
16		1.40 (-3)			
20	1.35 (-3)	1.19 (-3)	1.34 (-3)	1.34 (-3)	1.46 (-3)
22		1.07 (-3)			
24		9.51 (-4)			
25	1.03 (-3)		1.02 (-3)	1.04 (-3)	1.13 (-3)
26		8.33 (-4)			
28		7.13 (-4)			
28.5	8.17 (-4)		7.97 (-4)		
28.7				7.78 (-4)	
29					8.11 (-4)
30		6.22 (-4)			
35		5.21 (-4)			
40		4.35 (-4)			
50		3.08 (-4)			
60		2.10 (-4)			
70 N		1.32 (-4)			

[a]See experimental program plan in Appendix A for description of configurations.
[b]Read: 8.12×10^{-4}.

Table 21. Spectrum of high-energy neutrons (>0.8 MeV) on centerline at 25 cm behind the lead slab (Item IIB): Run 7941

Neutron Energy (MeV)	Flux (neutrons $cm^{-2}MeV^{-1}kW^{-1}s^{-1}$) Lower Limit	Upper Limit	Neutron Energy (MeV)	Flux (neutrons $cm^{-2}MeV^{-1}kW^{-1}s^{-1}$) Lower Limit	Upper Limit
8.11E -01	4.99E +02	5.06E +02	5.94E +00	1.32E +01	1.37E +01
9.07E -01	5.47E +02	5.51E +02	6.25E +00	1.15E +01	1.22E +01
1.01E +00	4.77E +02	4.81E +02	6.55E +00	9.96E +00	1.05E +01
1.11E +00	3.74E +02	3.77E +02	6.84E +00	8.67E +00	9.08E +00
1.20E +00	2.91E +02	2.93E +02	7.24E +00	7.02E +00	7.34E +00
1.31E +00	2.37E +02	2.39E +02	7.74E +00	5.19E +00	5.60E +00
1.41E +00	2.11E +02	2.13E +02	8.24E +00	3.73E +00	4.16E +00
1.51E +00	1.99E +02	2.01E +02	8.76E +00	2.97E +00	3.18E +00
1.61E +00	1.90E +02	1.92E +02	9.26E +00	2.53E +00	2.72E +00
1.71E +00	1.80E +02	1.82E +02	9.74E +00	1.99E +00	2.14E +00
1.81E +00	1.69E +02	1.71E +02	1.03E +01	1.36E +00	1.50E +00
1.93E +00	1.59E +02	1.60E +02	1.08E +01	9.44E -01	1.06E +00
2.10E +00	1.43E +02	1.45E +02	1.12E +01	7.63E -01	8.52E -01
2.30E +00	1.22E +02	1.24E +02	1.18E +01	5.76E -01	6.47E -01
2.50E +00	9.94E +01	1.01E +02	1.24E +01	3.16E -01	3.83E -01
2.70E +00	7.84E +01	7.98E +01	1.32E +01	1.68E -01	2.09E -01
2.90E +00	6.40E +01	6.54E +01	1.40E +01	1.05E -01	1.43E -01
3.10E +00	5.38E +01	5.53E +01	1.48E +01	3.75E -02	6.66E -02
3.30E +00	4.61E +01	4.73E +01	1.56E +01	1.37E -02	3.84E -02
3.50E +00	4.05E +01	4.18E +01	1.65E +01	1.09E -02	2.89E -02
3.71E +00	3.67E +01	3.76E +01	1.75E +01	1.54E -03	1.49E -02
3.91E +00	3.39E +01	3.48E +01	1.85E +01	-2.27E -03	9.17E -03
4.15E +00	3.15E +01	3.24E +01	1.95E +01	3.94E -03	5.73E -03
4.45E +00	2.80E +01	2.87E +01	2.05E +01	-1.18E -02	3.04E -03
4.75E +00	2.34E +01	2.41E +01	2.16E +01	-1.24E -02	3.19E -03
5.04E +00	1.95E +01	2.01E +01	2.26E +01	-5.55E -03	4.66E -03
5.34E +00	1.66E +01	1.71E +01	2.35E +01	-2.97E -03	6.02E -03
5.64E +00	1.47E +01	1.53E +01			

E1 (MeV)	E2 (MeV)	Integral neutrons $cm^{-2}kW^{-1}s^{-1}$	Error neutrons $cm^{-2}kW^{-1}s^{-1}$
0.811	1.000	1.00E +02	4.09E -01
1.000	1.200	7.69E +01	3.07E -01
1.200	1.600	8.95E +01	5.10E -01
1.600	2.000	6.88E +01	3.99E -01
2.000	3.000	1.02E +02	7.66E -01
3.000	4.000	4.28E +01	5.82E -01
4.000	6.000	4.34E +01	6.52E -01
6.000	8.000	1.68E +01	4.55E -01
8.000	10.000	5.87E +00	2.36E -01
10.000	12.000	1.94E +00	1.03E -01
12.000	16.000	6.04E -01	7.92E -02
16.000	20.000	3.24E -02	2.68E -02
3.000	10.000	1.09E +02	1.93E +00
1.500	15.000	3.02E +02	3.38E +00
3.000	12.000	1.11E +02	2.03E +00

Table 22. Neutron spectrum (50 keV to 1.4 MeV) on centerline at 25 cm behind the lead slab (Item IIB) Runs 1611.C, 1611.B, 1611.A

N	Energy Boundary (MeV)		Flux (neutrons $cm^{-2}MeV^{-1}kW^{-1}s^{-1}$)	Error (%)
		RUN 1611.C		
1	0.0397	0.0450	4.63E +03	2.16
2	0.0450	0.0538	3.92E +03	2.30
3	0.0538	0.0626	3.88E +03	2.61
4	0.0626	0.0732	3.82E +03	2.43
5	0.0732	0.0873	3.15E +03	2.37
6	0.0873	0.1014	1.92E +03	4.44
7	0.1014	0.1208	2.00E +03	3.32
8	0.1208	0.1419	2.28E +03	3.02
9	0.1419	0.1666	1.61E +03	4.01
10	0.1666	0.1966	1.41E +03	4.09
		RUN 1611.B		
1	0.1433	0.1699	1.58E +03	1.68
2	0.1699	0.1966	1.32E +03	2.31
3	0.1966	0.2299	1.23E +03	2.26
4	0.2299	0.2766	1.25E +03	1.77
5	0.2766	0.3232	1.18E +03	2.20
6	0.3232	0.3765	9.60E +02	2.65
7	0.3765	0.4432	7.69E +02	2.93
8	0.4432	0.5231	8.31E +02	2.51
9	0.5231	0.6164	8.26E +02	2.36
10	0.6164	0.7297	7.17E +02	2.35
		RUN 1611.A		
1	0.5243	0.6216	7.82E +02	1.57
2	0.6216	0.7297	6.89E +02	1.76
3	0.7297	0.8595	6.07E +02	1.76
4	0.8595	1.0108	4.84E +02	1.99
5	1.0108	1.1838	3.30E +02	2.66
6	1.1838	1.4000	2.18E +02	3.29

Table 23. Spectrum of high-energy neutrons (>0.8 MeV) on centerline at 25 cm behind the lead slab (Item IIIA): Run 7939

Neutron Energy (MeV)	Flux (neutrons $cm^{-2}MeV^{-1}kW^{-1}s^{-1}$) Lower Limit	Upper Limit	Neutron Energy (MeV)	Flux (neutrons $cm^{-2}MeV^{-1}kW^{-1}s^{-1}$) Lower Limit	Upper Limit
8.11E -01	3.61E +02	3.68E +02	5.94E +00	1.00E +01	1.04E +01
9.07E -01	3.93E +02	3.96E +02	6.25E +00	8.44E +00	8.89E +00
1.01E +00	3.46E +02	3.48E +02	6.55E +00	7.41E +00	7.78E +00
1.11E +00	2.70E +02	2.72E +02	6.84E +00	6.57E +00	6.85E +00
1.20E +00	2.06E +02	2.08E +02	7.24E +00	5.48E +00	5.69E +00
1.31E +00	1.64E +02	1.66E +02	7.74E +00	4.22E +00	4.51E +00
1.41E +00	1.45E +02	1.47E +02	8.24E +00	3.27E +00	3.58E +00
1.51E +00	1.36E +02	1.38E +02	8.76E +00	2.61E +00	2.75E +00
1.61E +00	1.30E +02	1.31E +02	9.26E +00	1.95E +00	2.08E +00
1.71E +00	1.22E +02	1.24E +02	9.74E +00	1.48E +00	1.57E +00
1.81E +00	1.16E +02	1.17E +02	1.03E +01	1.15E +00	1.24E +00
1.93E +00	1.09E +02	1.10E +02	1.08E +01	9.14E -01	9.94E -01
2.10E +00	9.81E +01	9.93E +01	1.12E +01	6.90E -01	7.51E -01
2.30E +00	8.20E +01	8.31E +01	1.18E +01	4.35E -01	4.83E -01
2.50E +00	6.51E +01	6.60E +01	1.24E +01	2.28E -01	2.75E -01
2.70E +00	5.17E +01	5.26E +01	1.32E +01	1.44E -01	1.74E -01
2.90E +00	4.39E +01	4.48E +01	1.40E +01	8.63E -02	1.12E -01
3.10E +00	3.86E +01	3.96E +01	1.48E +01	4.91E -02	6.94E -02
3.30E +00	3.37E+ 01	3.44E +01	1.56E +01	2.42E -02	4.14E -02
3.50E +00	2.97E +01	3.06E +01	1.65E +01	9.32E -03	2.11E -02
3.71E +00	2.72E +01	2.78E +01	1.75E +01	-2.25E -03	6.29E -03
3.91E +00	2.51E +01	2.57E +02	1.85E +01	-4.17E -03	3.42E -03
4.15E +00	2.31E +01	2.36E +01	1.95E +01	-2.48E -03	3.62E -03
4.45E +00	2.07E +01	2.12E +01	2.05E +01	-6.18E -03	3.10E -03
4.75E +00	1.78E +01	1.82E +01	2.16E +01	-6.88E -03	2.87E -03
5.04E +00	1.51E +01	1.55E +01	2.26E +01	-3.33E -03	2.99E -03
5.34E +00	1.32E +01	1.36E +01	2.35E +01	-2.00E -03	3.57E -03
5.64E +00	1.16E +01	1.21E +01			

E1 (MeV)	E2 (MeV)	Integral neutrons $cm^{-2}kW^{-1}s^{-1}$	Error neutrons $cm^{-2}kW^{-1}s^{-1}$
0.811	1.000	7.22E +01	2.95E -01
1.000	1.200	5.56E +01	1.91E -01
1.200	1.600	6.18E +01	3.24E -01
1.600	2.000	4.70E +01	2.64E -01
2.000	3.000	6.86E +01	4.95E -01
3.000	4.000	3.13E +01	3.84E -01
4.000	6.000	3.30E +01	4.34E -01
6.000	8.000	1.28E +01	3.09E -01
8.000	10.000	4.84E +00	1.65E -01
10.000	12.000	1.67E +00	7.08E -02
12.000	16.000	4.94E -01	5.49E -02
16.000	20.000	1.85E -02	1.74E -02
3.000	10.000	8.18E +01	1.30E +00
1.500	15.000	2.13E +02	2.25E +00
3.000	12.000	8.35E +01	1.37E +00

Table 24. Neutron spectrum (50 keV to 1.4 MeV) on centerline at 25 cm behind the lead slab (Item IIIA) Runs 1609.C, 1609.B, 1609.A

N	Energy Boundary (MeV)		Flux (neutrons $cm^{-2}MeV^{-1}kW^{-1}s^{-1}$)	Error (%)
		RUN 1609.C		
1	0.0396	0.0449	3.43E +03	4.03
2	0.0449	0.0537	3.09E +03	3.00
3	0.0537	0.0626	3.09E +03	3.39
4	0.0626	0.0749	3.08E +03	2.61
5	0.0749	0.0872	2.31E +03	3.89
6	0.0872	0.1031	1.46E +03	5.20
7	0.1031	0.1207	1.63E +03	4.72
8	0.1207	0.1419	1.82E +03	3.83
9	0.1419	0.1683	1.28E +03	4.67
10	0.1683	0.1982	1.06E +03	5.51
		RUN 1609.B		
1	0.1445	0.1714	1.23E +03	1.66
2	0.1714	0.1982	9.86E +02	2.39
3	0.1982	0.2318	9.10E +02	2.35
4	0.2318	0.2722	9.64E +02	2.08
5	0.2722	0.3259	9.28E +02	1.80
6	0.3259	0.3797	7.35E +02	2.63
7	0.3797	0.4469	5.45E +02	3.11
8	0.4469	0.5275	5.75E +02	2.72
9	0.5275	0.6216	5.74E +02	2.52
		RUN 1609.A		
1	0.4486	0.5243	5.21E +02	1.93
2	0.5243	0.6216	5.50E +02	1.53
3	0.6216	0.7297	4.83E +02	1.72
4	0.7297	0.8595	4.21E +02	1.74
5	0.8595	1.0108	3.51E +02	1.88
6	1.0108	1.1838	2.36E +02	2.53
7	1.1838	1.4000	1.50E +02	3.25

APPENDIX C

FIGURES

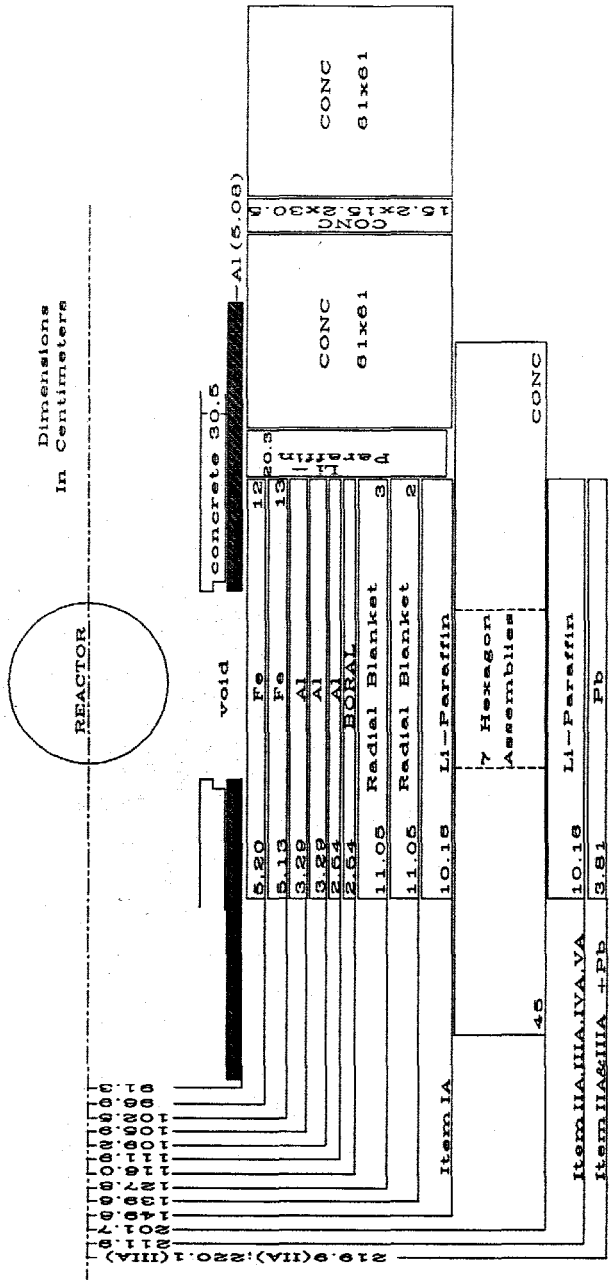

Figure 1. Schematic of the axial shield mockup plus lead slab (Items IA, IIA, IIIA, IVA, VA, IIA and IIIA + Pb slab).
Note: Lithiated paraffin covers four sides of the SM-1.

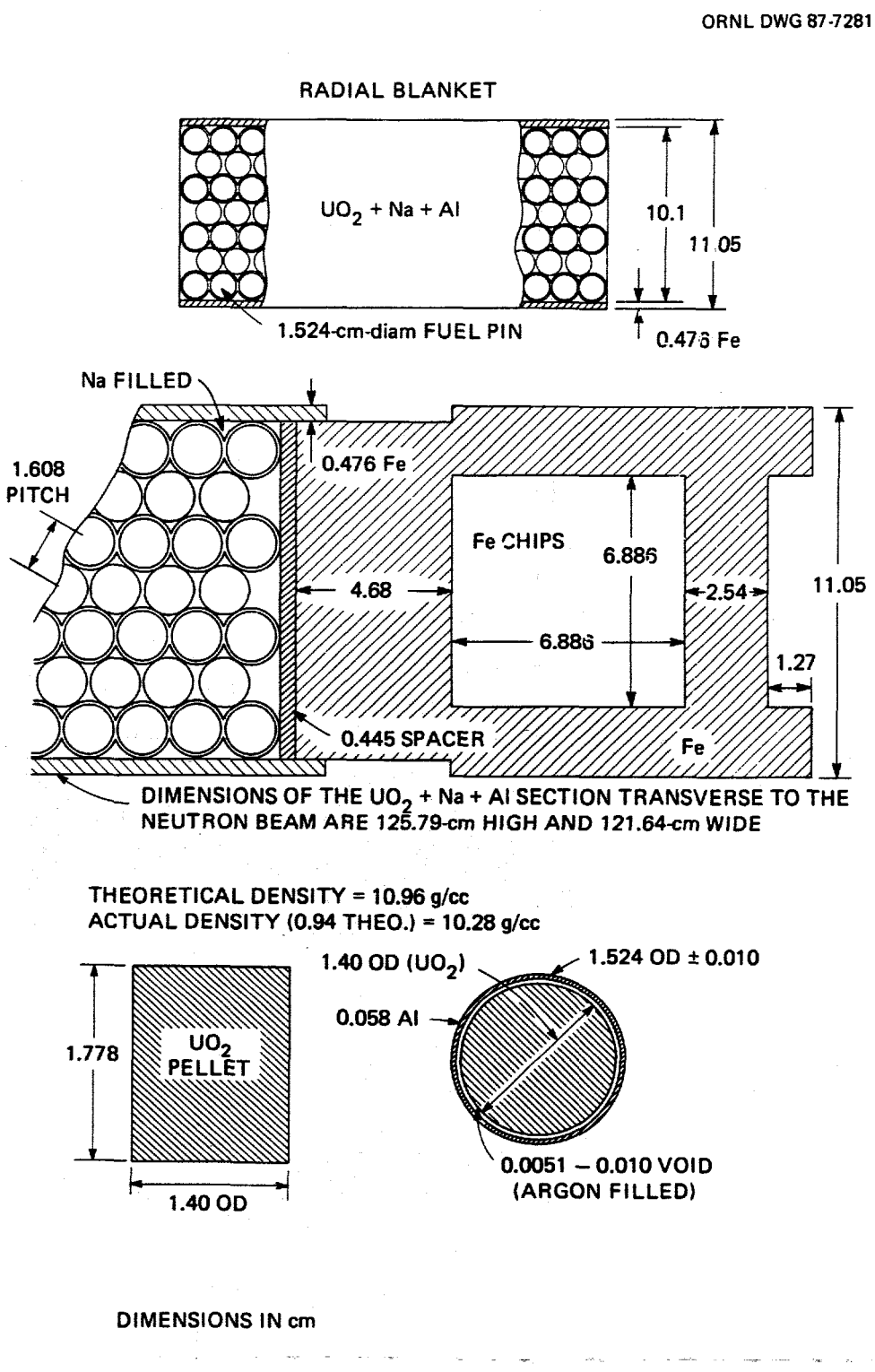

Figure 2. Schematic of radial blanket slab containing UO_2.

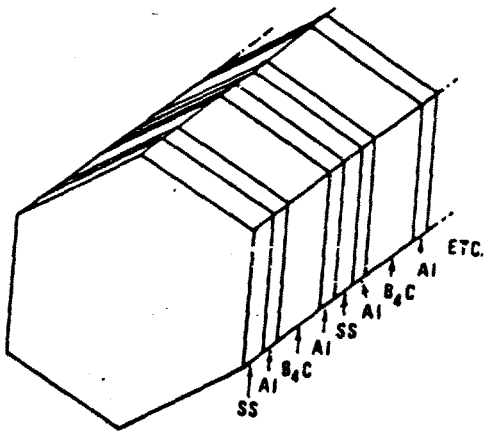

Depth of B_4C in container: 7.77 cm (4 total)
Width of B_4C: 14.73 cm
End plate thickness: 1.123 cm
Wall thickness of container: 0.627 cm
Width of container (flat surface to flat surface: 15.98 cm
Density of B_4C: 1.41 g/cc
Thickness of SS pieces: 1.25 cm (4 total)

Figure 3. B_4C homogeneous-type assembly.

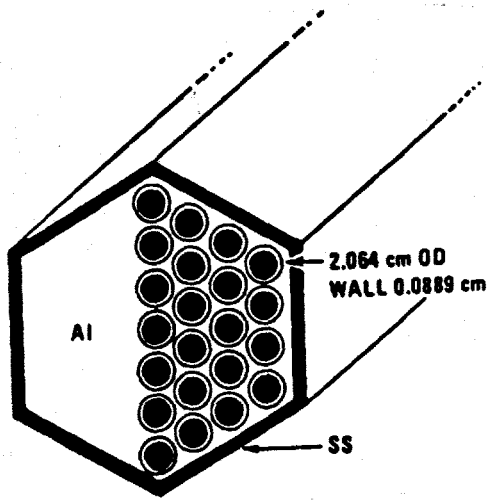

OD of rod: 2.06 cm
ID of rod wall: 1.897 cm
Rod wall thickness: 0.0813 cm
Thickness of rod cap: 0.159 cm
Length of B_4C in rod: 44.7 cm
Volume of B_4C rod: 126.28 cc
Average density of B_4C: 1.30 g/cc
Thickness of SS wrapper: 0.465 cm
Rod pitch: 2.38 cm
Width of Al (flat surface to flat surface): 15.00 cm
Width of assembly (flat surface to flat surface): 15.93 cm

Figure 4. B_4C rod bundle assembly (37 tubes).

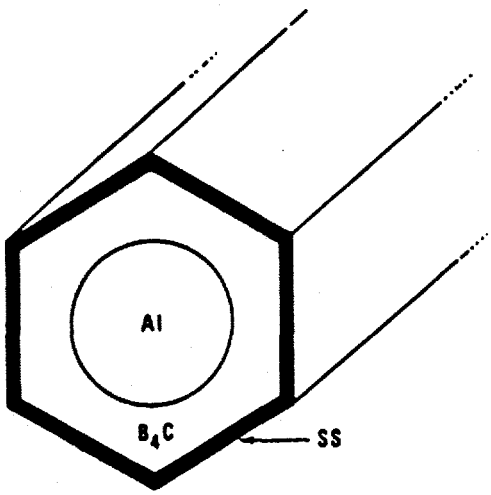

Diam of Al cylinder: 8.96 cm
Length of Al cylinder: 43.412 cm
Width of hexagon (flat surface to flat surface): 15.99 cm
Thickness of SS wrapper: 0.452 cm
Length of SS wrapper: 45 cm
Volume of B_4C: 5760.1 cc
Density of B_4C: 1.39 g/cc
Thickness of Al covers over end of B_4C: 0.794 cm

Figure 5. B_4C central Na channel assembly.

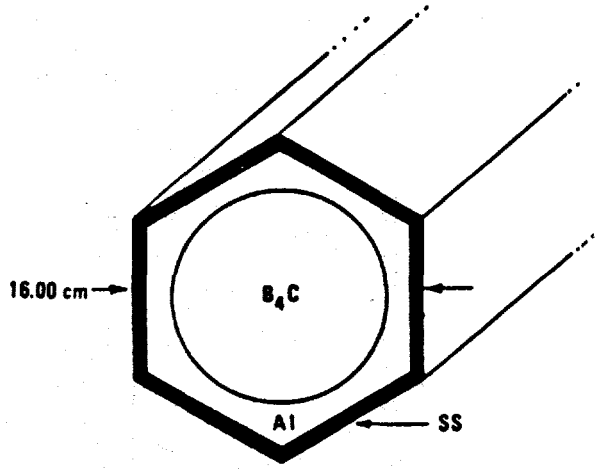

Width of container (flat surface to flat surface): 16.00 cm
Width of Al (flat surface to flat surface): 15.05 cm
Thickness of end plates: 0.476 cm
Diam of B_4C: 13 cm
Length of B_4C: 44.05 cm
Volume of B_4C: 5846.9 cc
Density of B_4C: 1.38 g/cc

Figure 6. B_4C central blockage hexagon assembly.

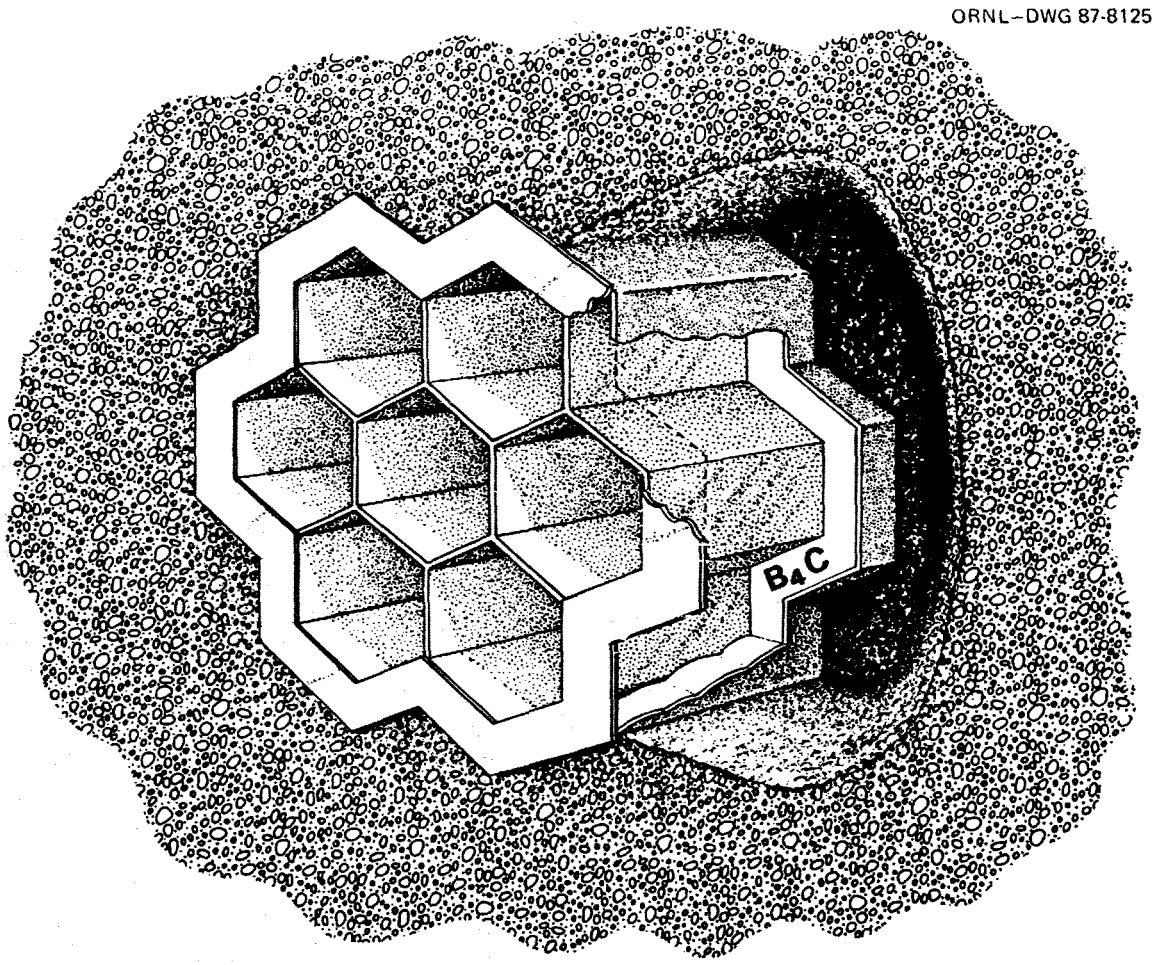

Figure 7. Schematic of the aluminum honeycomb within a concrete slab.

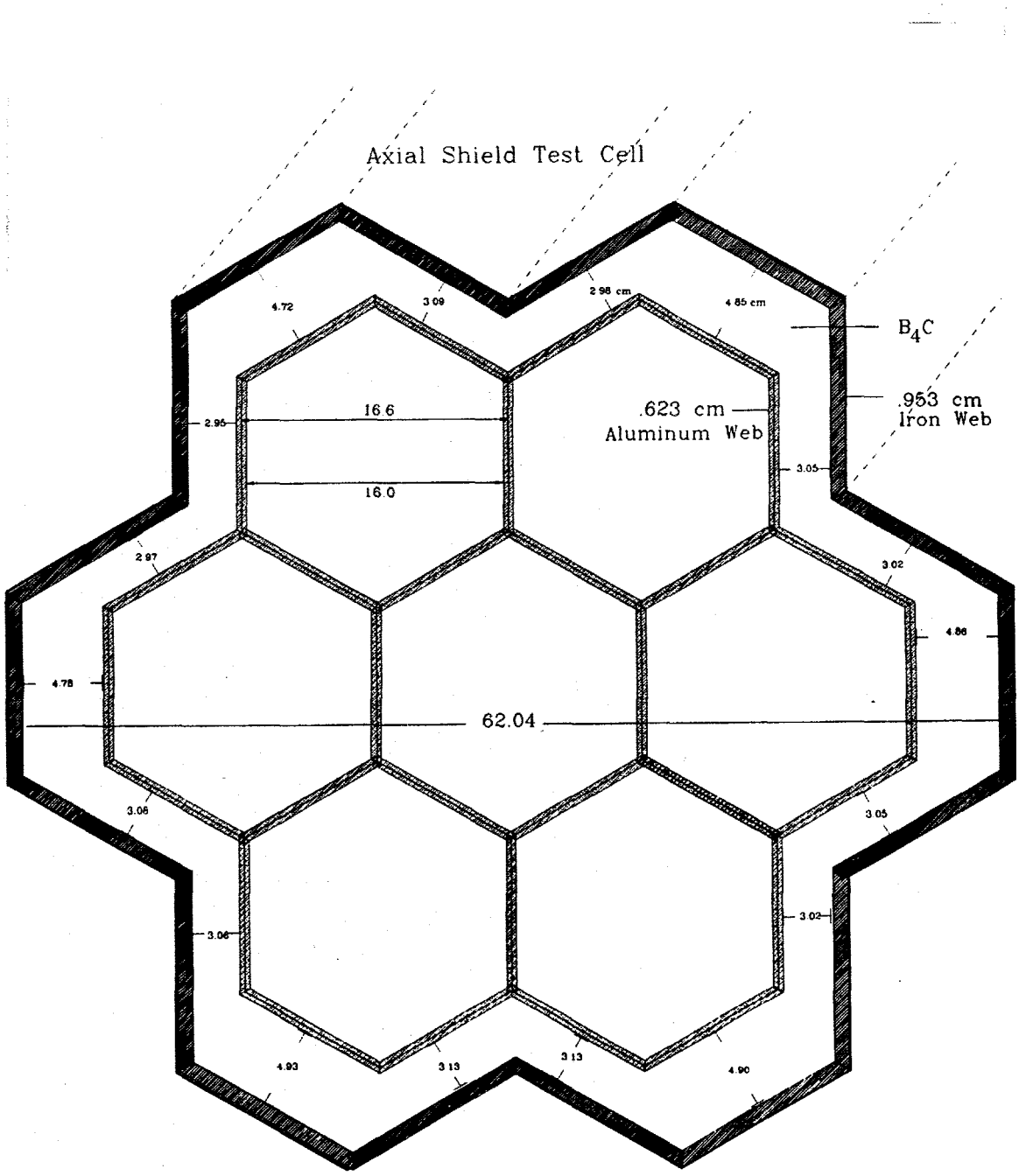

Figure 8. Schematic of aluminum mesh dimensions along with those for the surrounding B_4C collar.

ORNL Photo No. 5114-87A

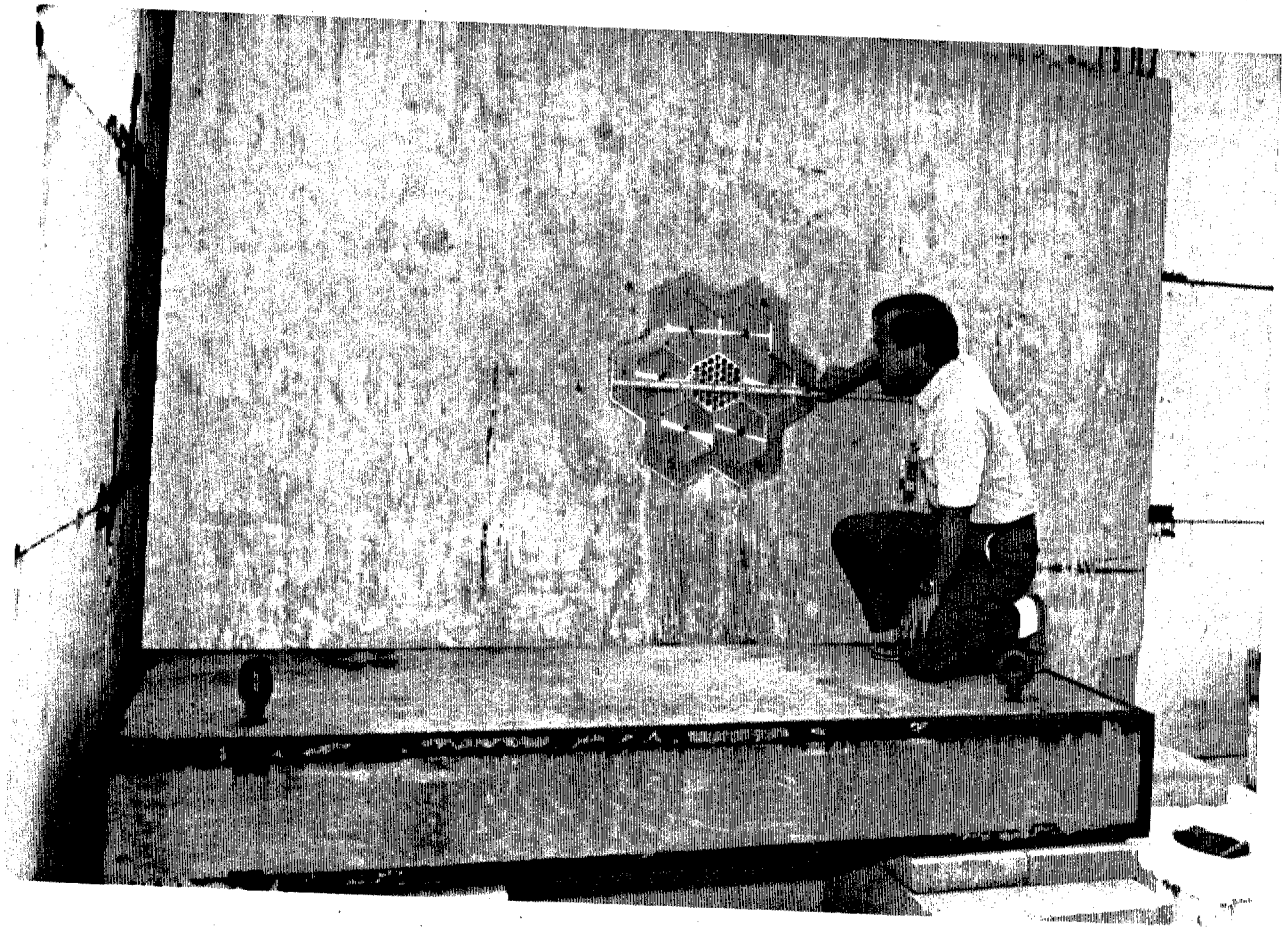

Figure 9. A photograph of a typical axial shield mockup.

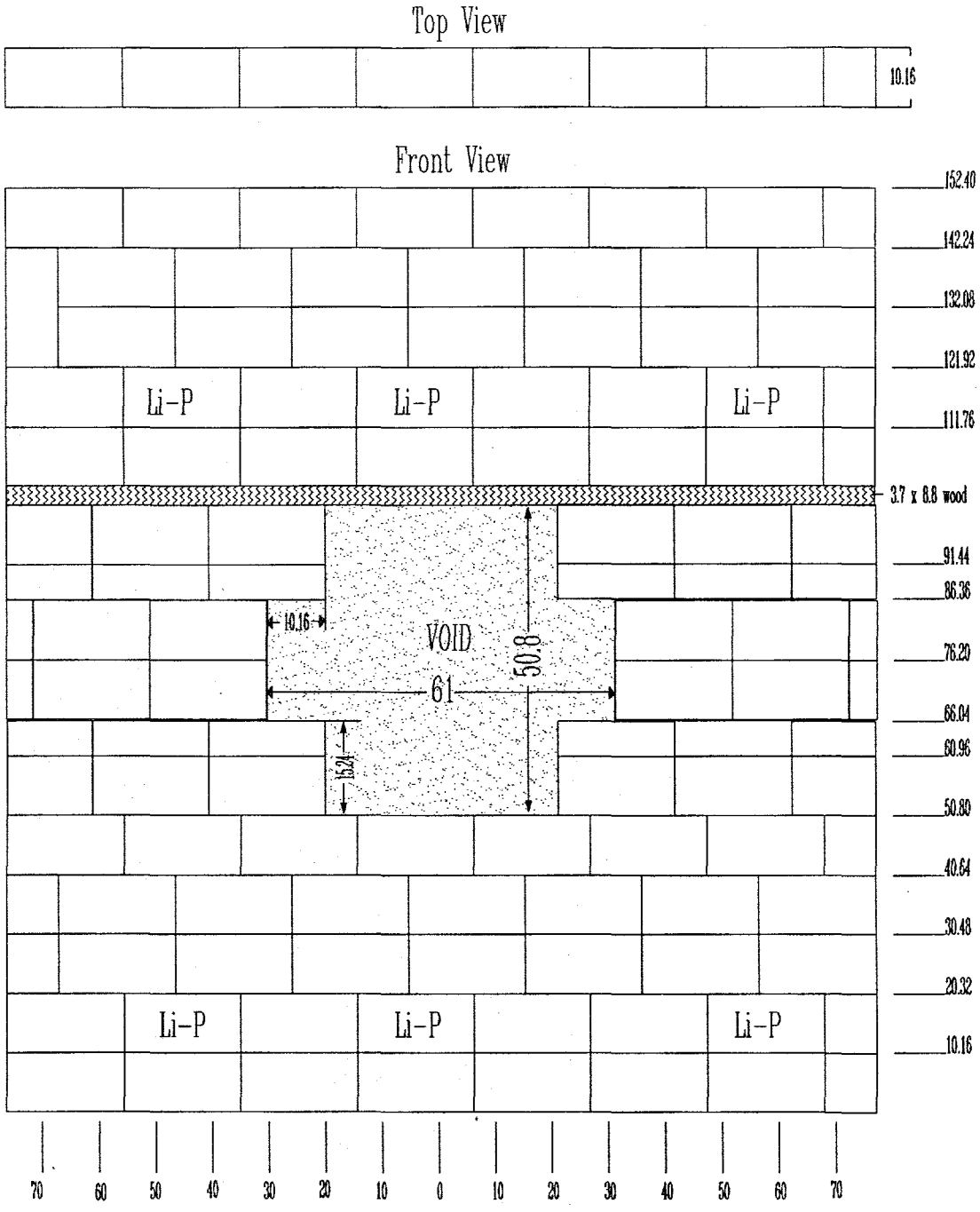

Figure 10. Schematic of the lithiated paraffin slabs with void.

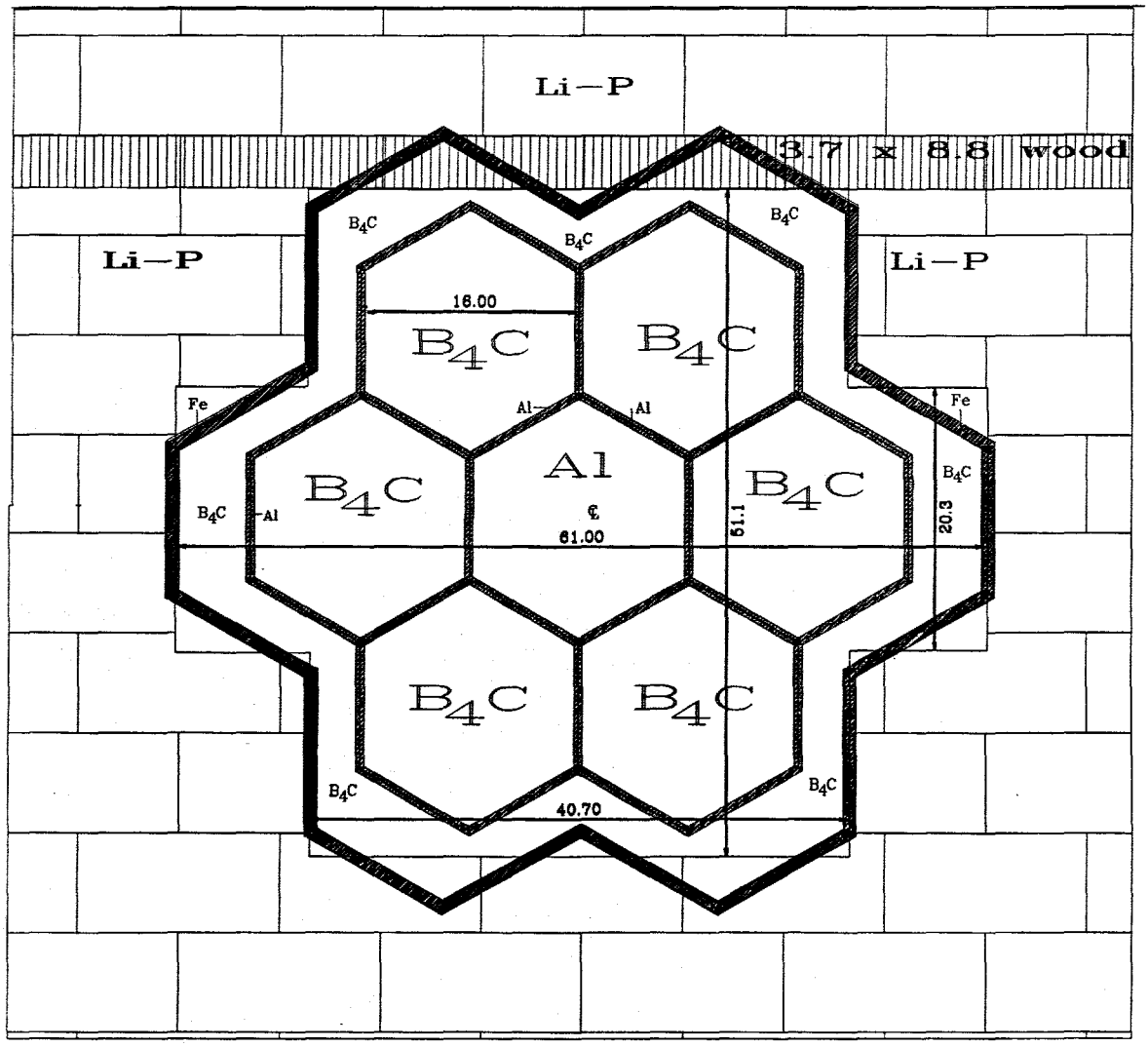

Figure 11. Schematic of the lithiated paraffin slab iris superimposed upon the seven-hexagon arrangement in the axial shield.

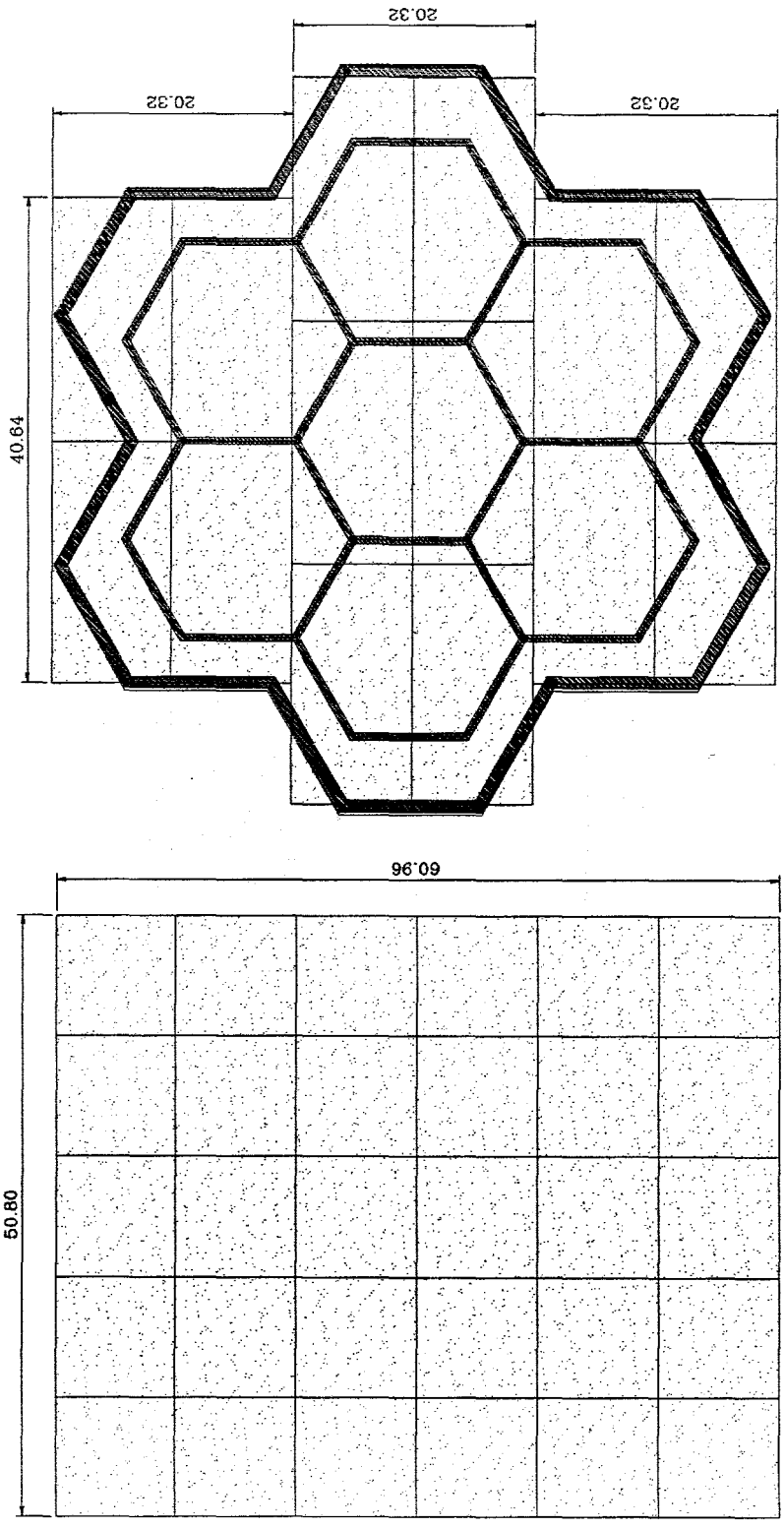

Figure 12. Lithiated paraffin background shield (shaded area) for the Axial Shield experiment.

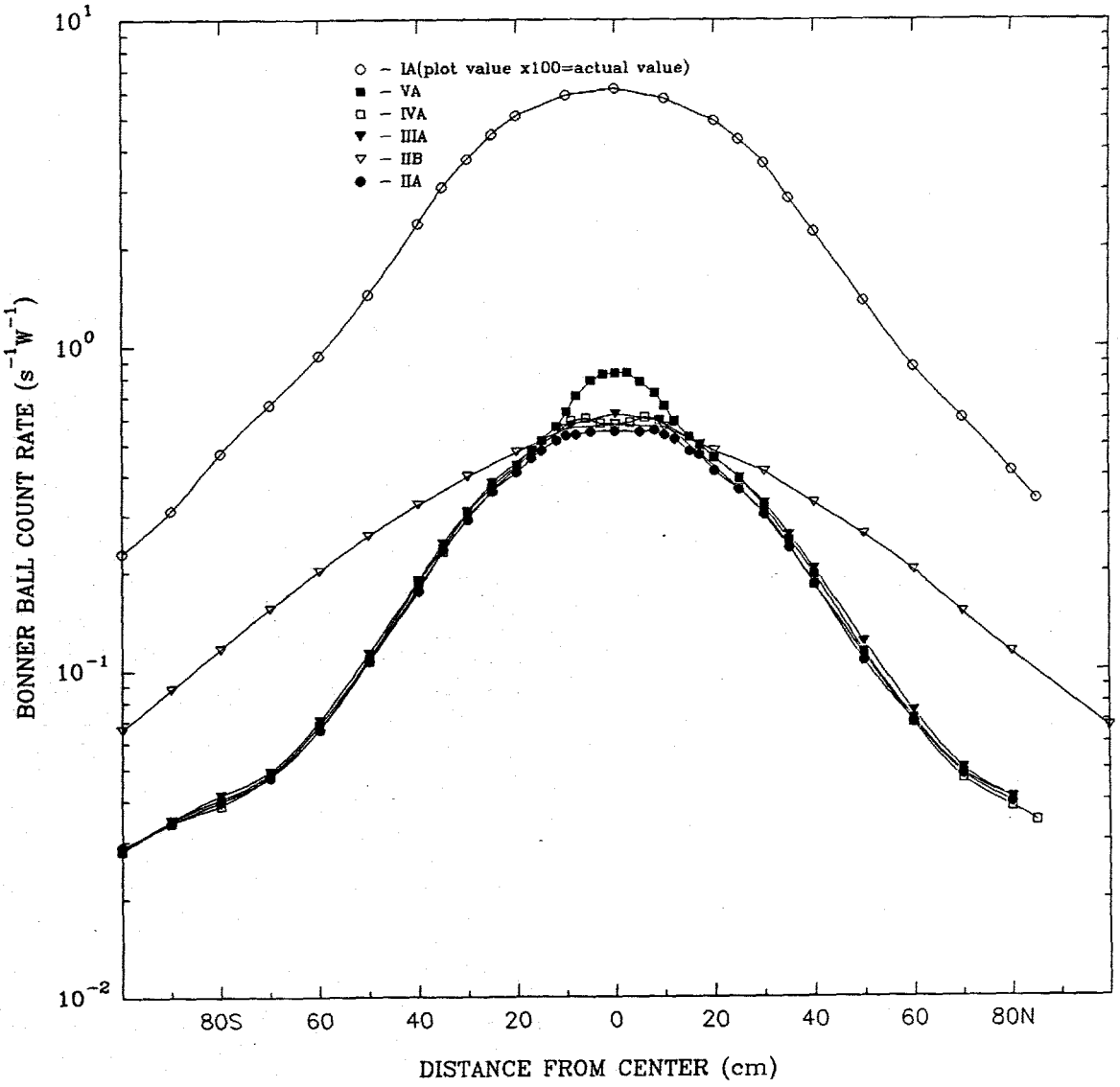

Figure 13. 3-inch Bonner ball traverses through the horizontal midplane at 30 cm behind a series of configurations (Items IA, IIA, IIB, IIIA, IVA, VA).

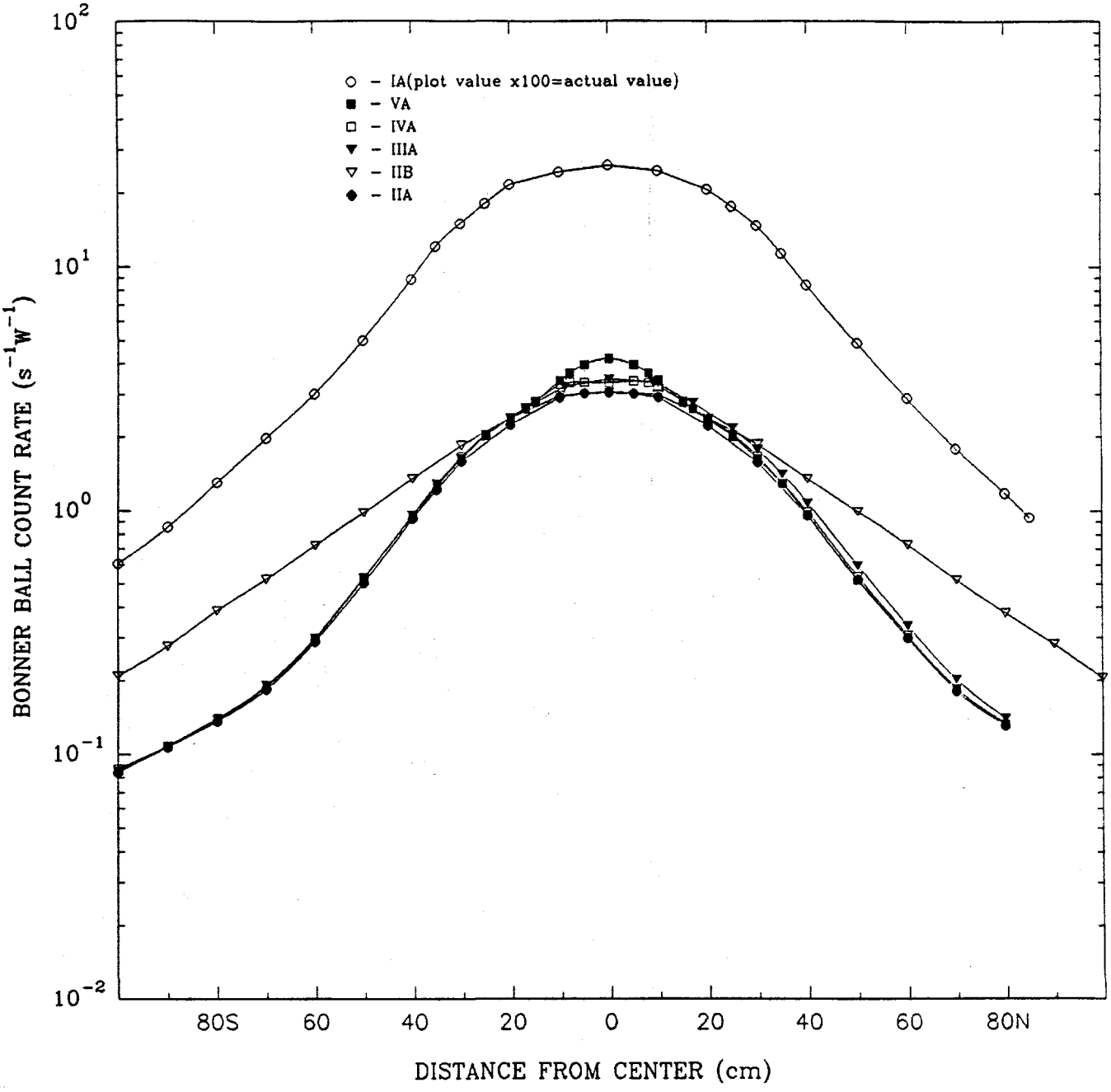

Figure 14. 5-inch Bonner ball traverses through the horizontal midplane at 30 cm behind a series of configurations (Items IA, IIA, IIB, IIIA, IVA, VA).

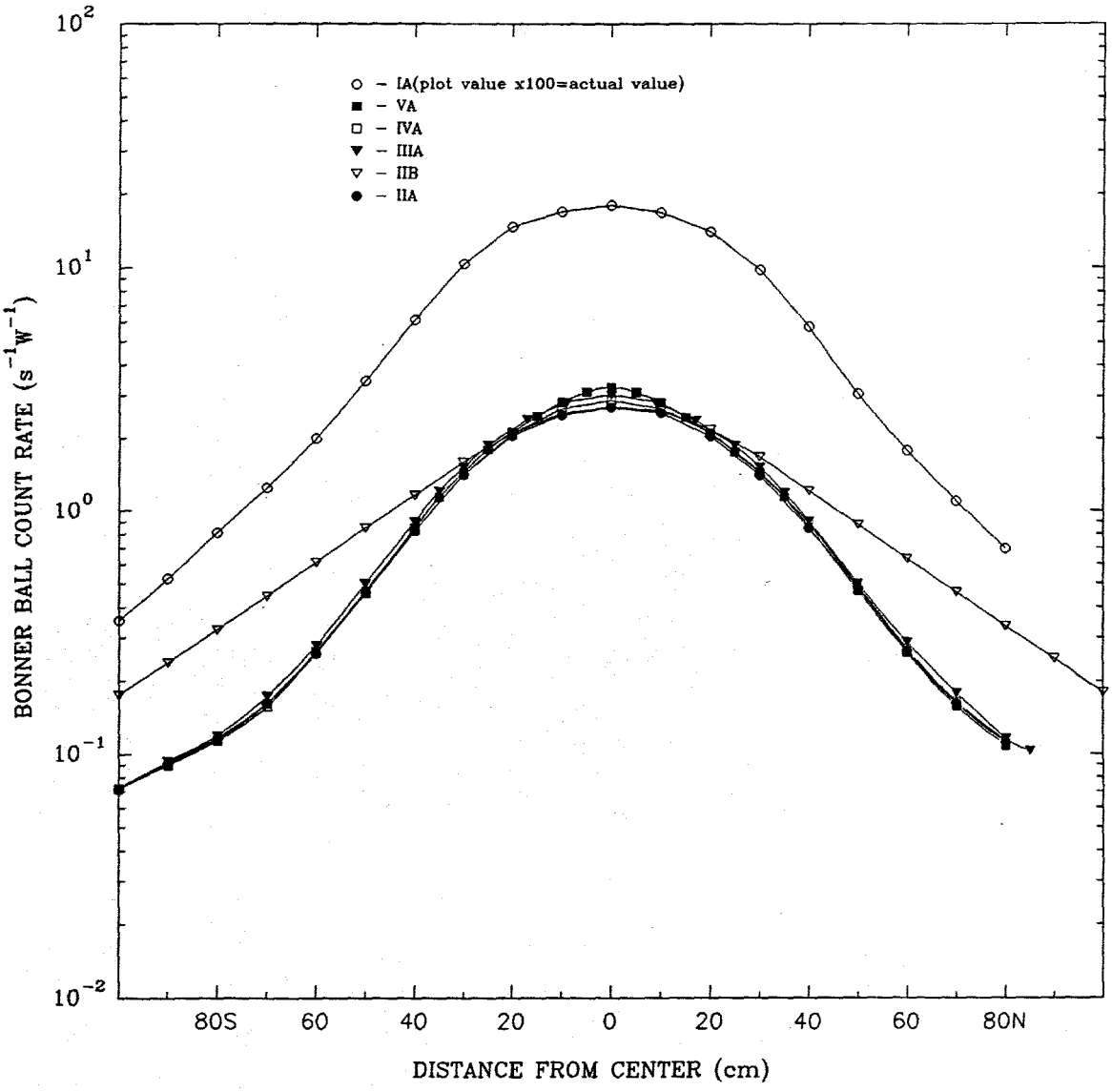

Figure 15. 8-inch Bonner ball traverses through the horizontal midplane at 30 cm behind a series of configurations (Items IA, IIA, IIB, IIIA, IVA, VA).

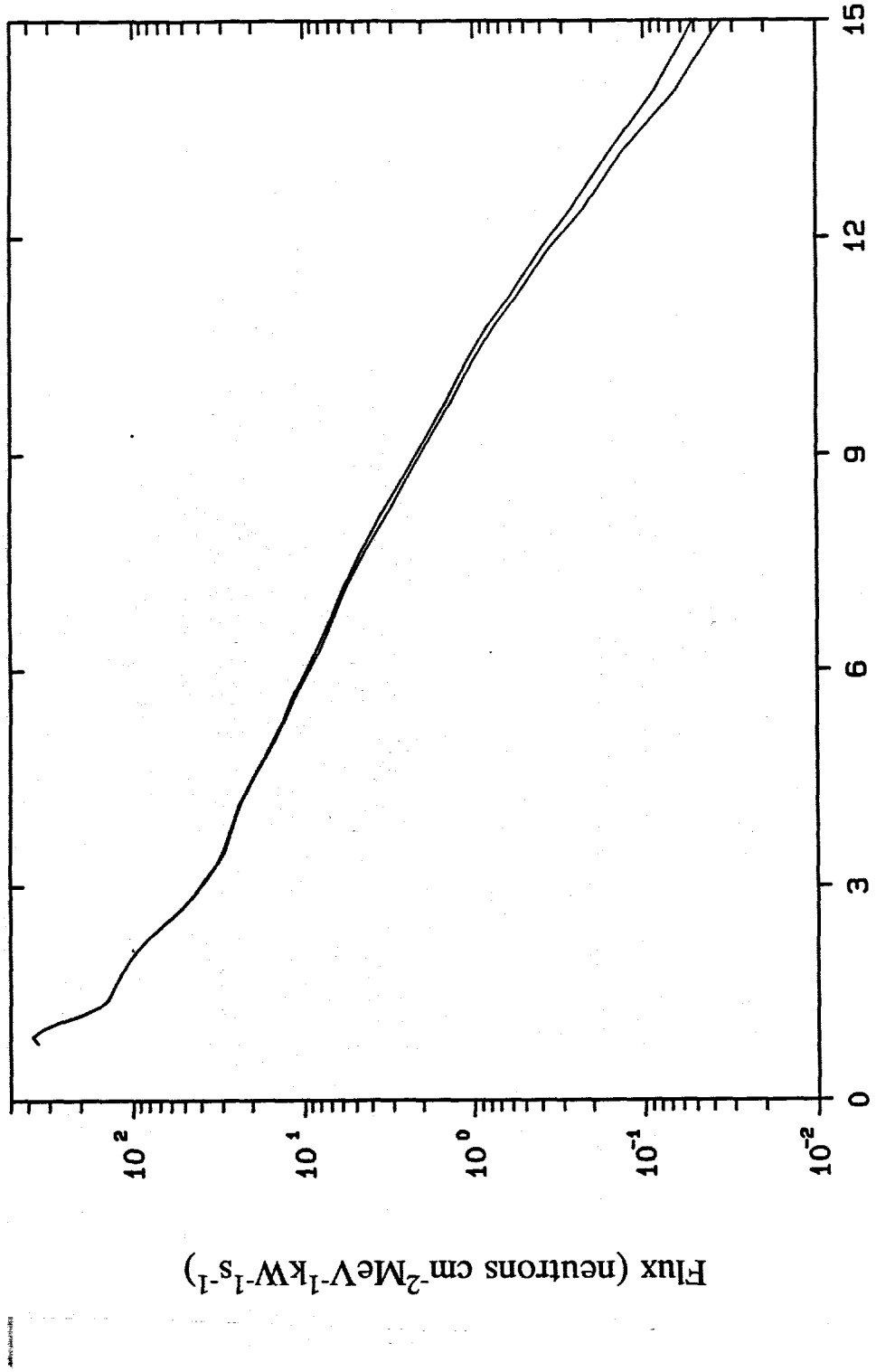

Figure 16. Spectrum of high-energy neutrons (>0.8 MeV) on centerline at 25 cm behind the lead slab (Item IIA) Run 7940.

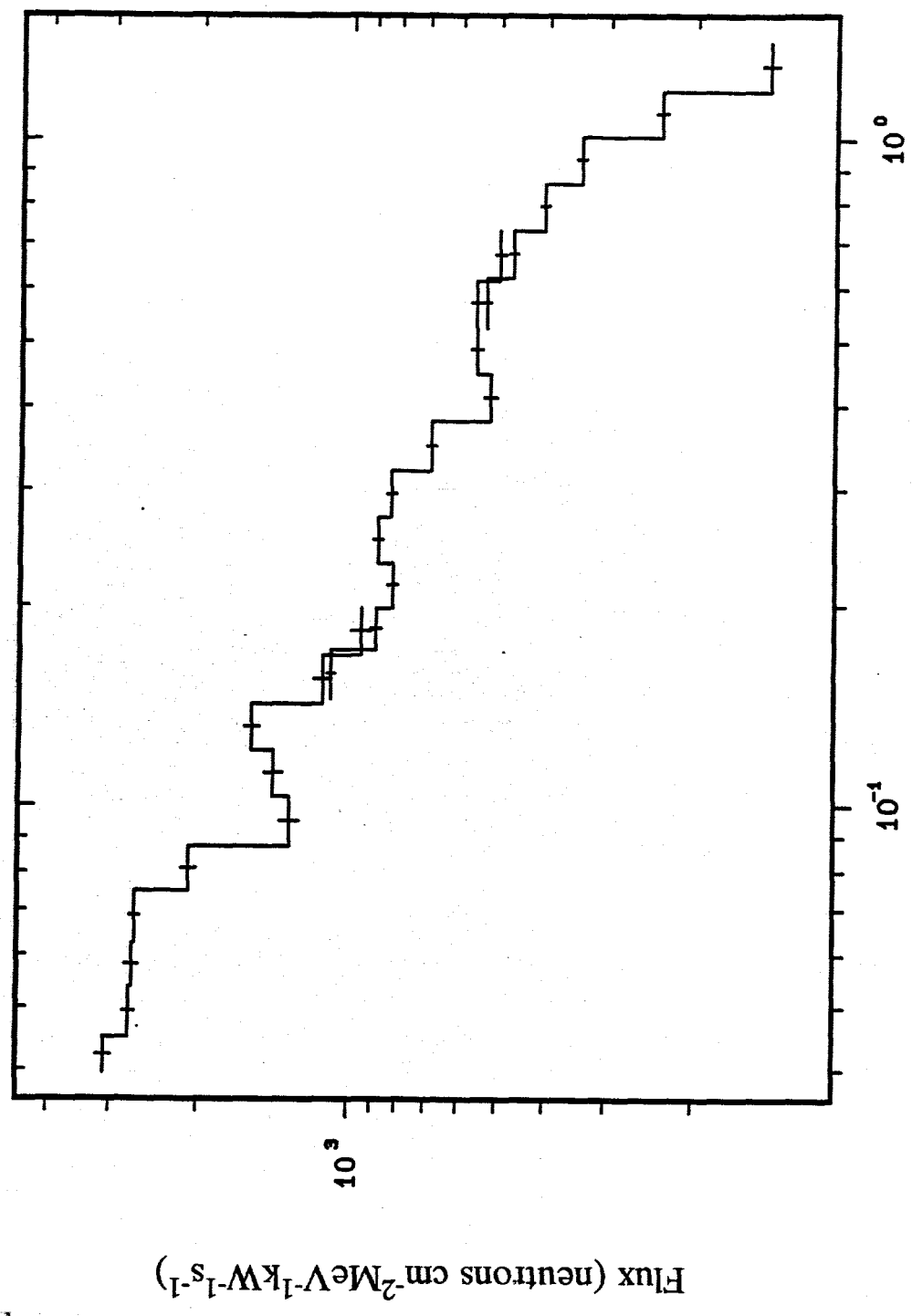

Figure 17. Neutron spectrum (50 keV to 1.4 MeV) on centerline at 25 cm behind the lead slab (Item IIA) Runs 1610B, 1610C, 1610A.

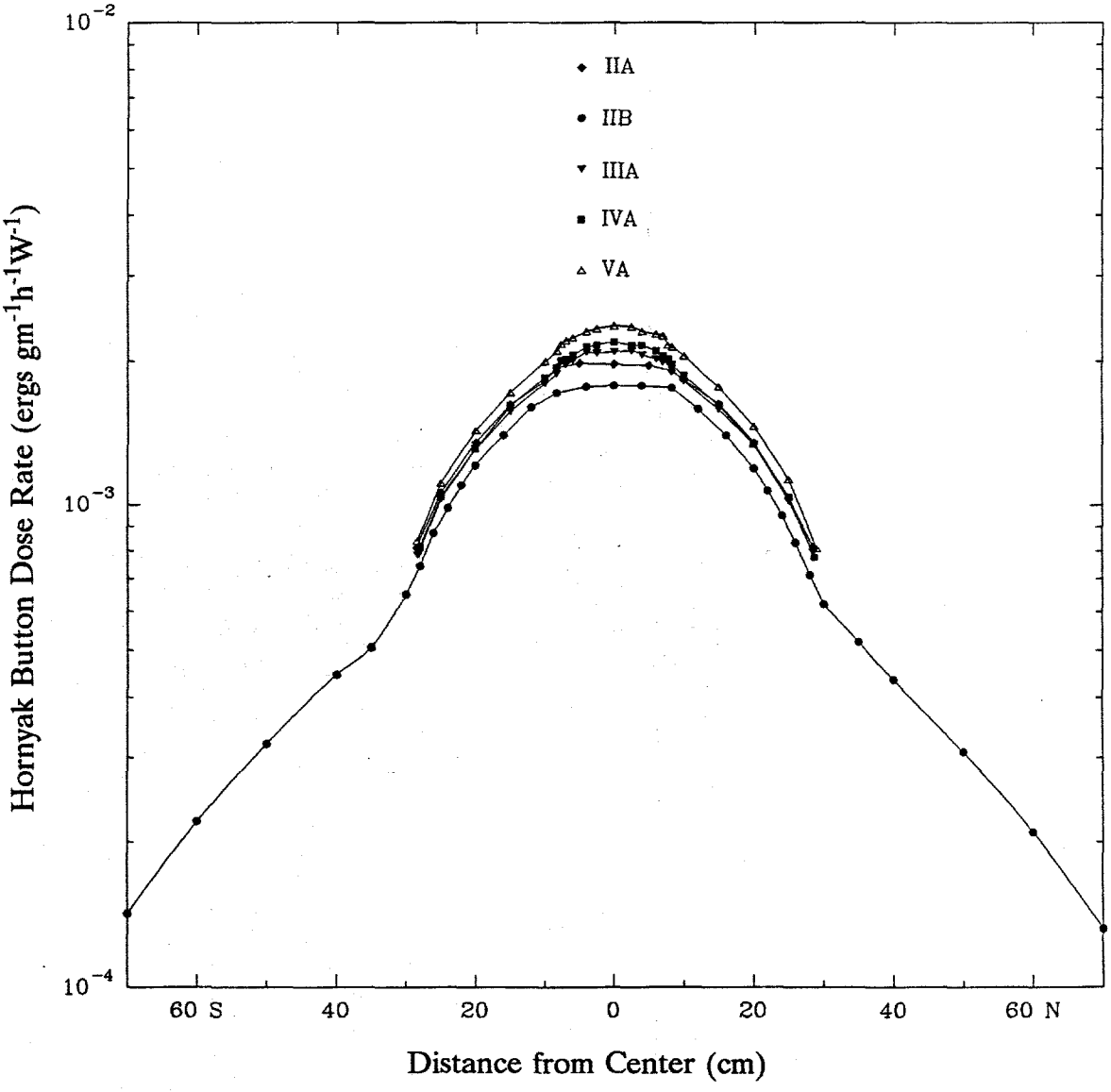

Figure 18. Radial traverses at 2.4 cm behind the axial shield in a series of configurations using the Hornyak button (Items IIA, IIB, IIIA, IVA, VA).

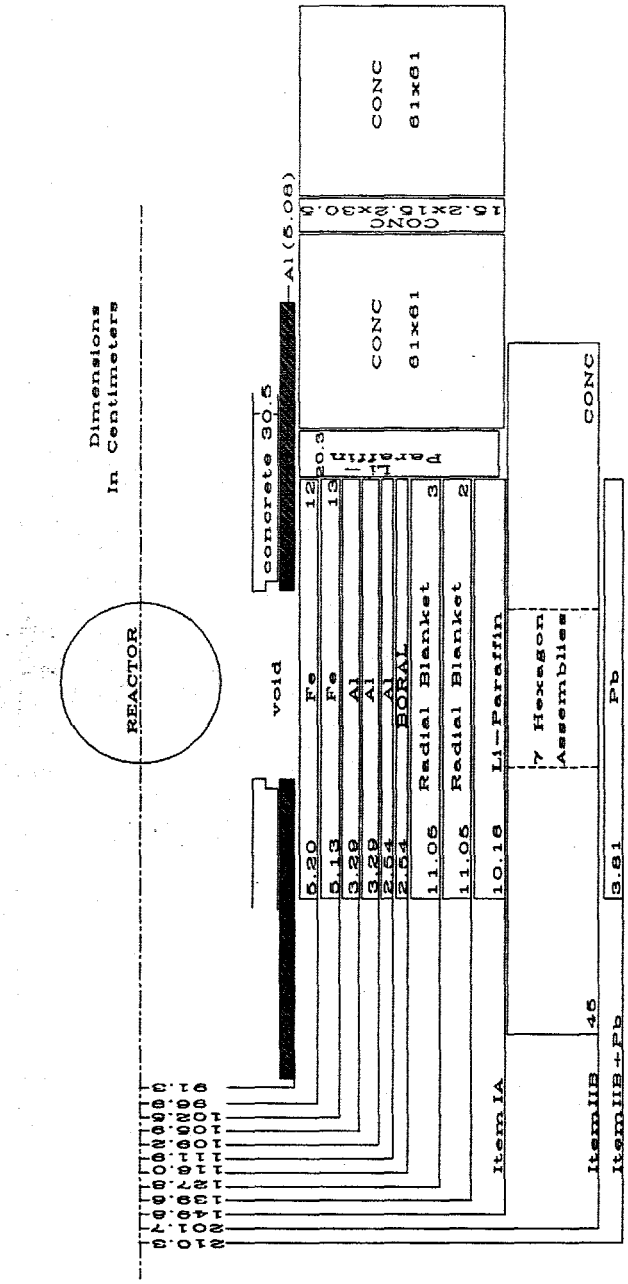

Figure 19. Schematic of the axial shield mockup plus lead slab (Items IA, IIB, IIB + Pb slab).

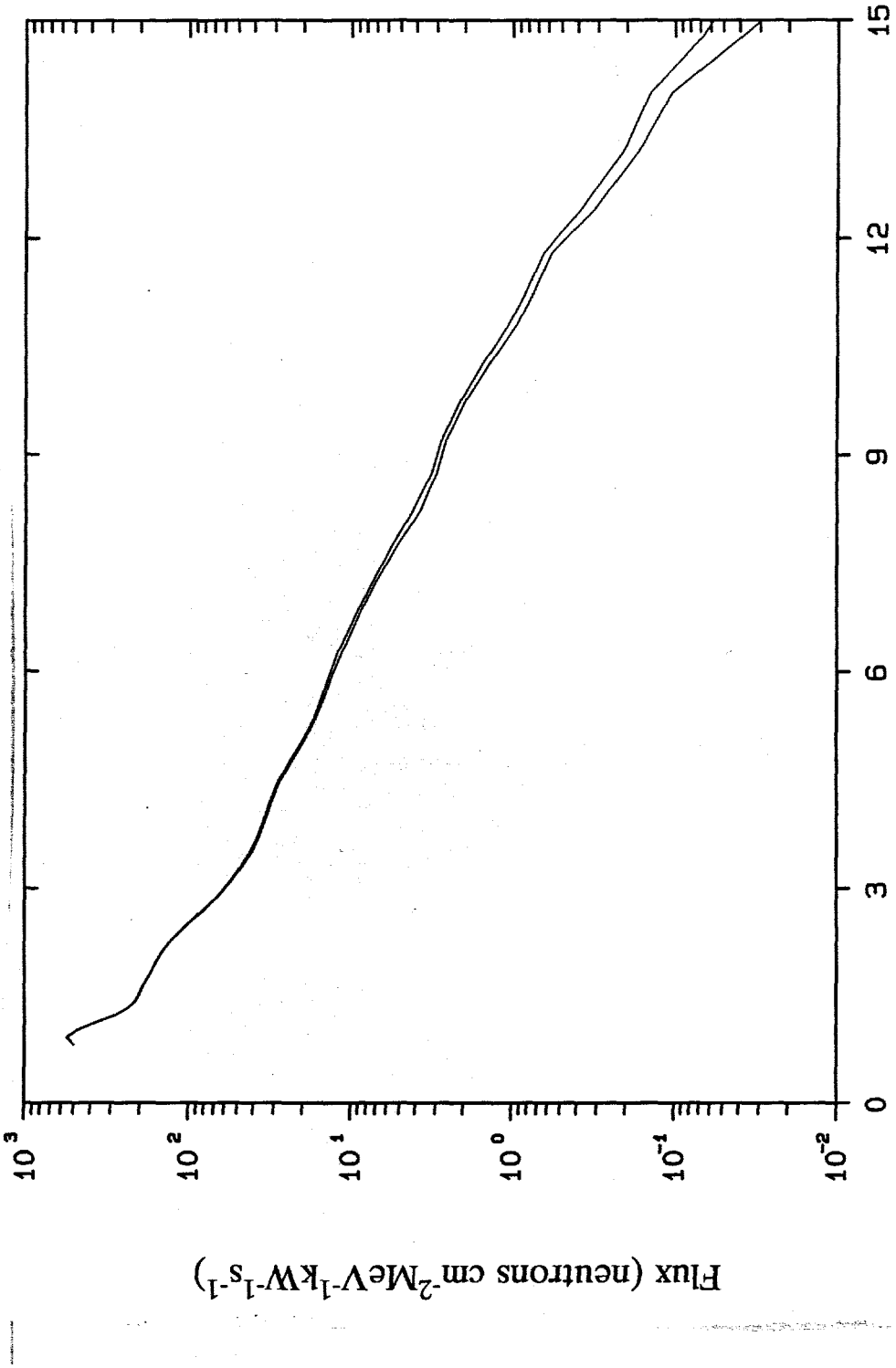

Figure 20. Spectrum of high-energy neutrons (>0.8 MeV) on centerline at 25 cm behind the lead slab (Item IIA) Run 7940.

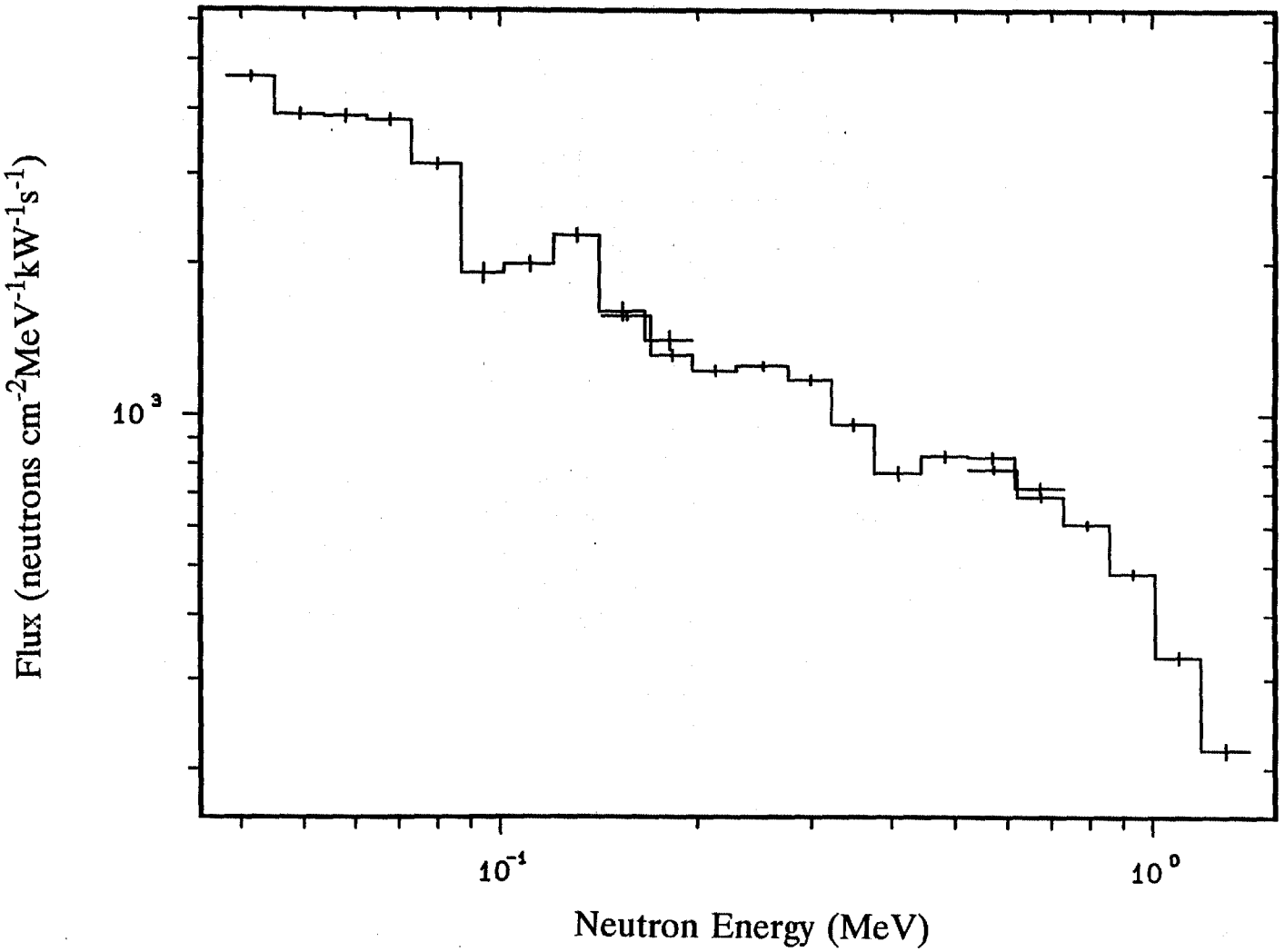

Figure 21. Neutron spectrum (50 keV to 1.4 MeV) on centerline at 25 cm behind the lead slab (Item IIB) Runs 1611C, 1611B, 1611A.

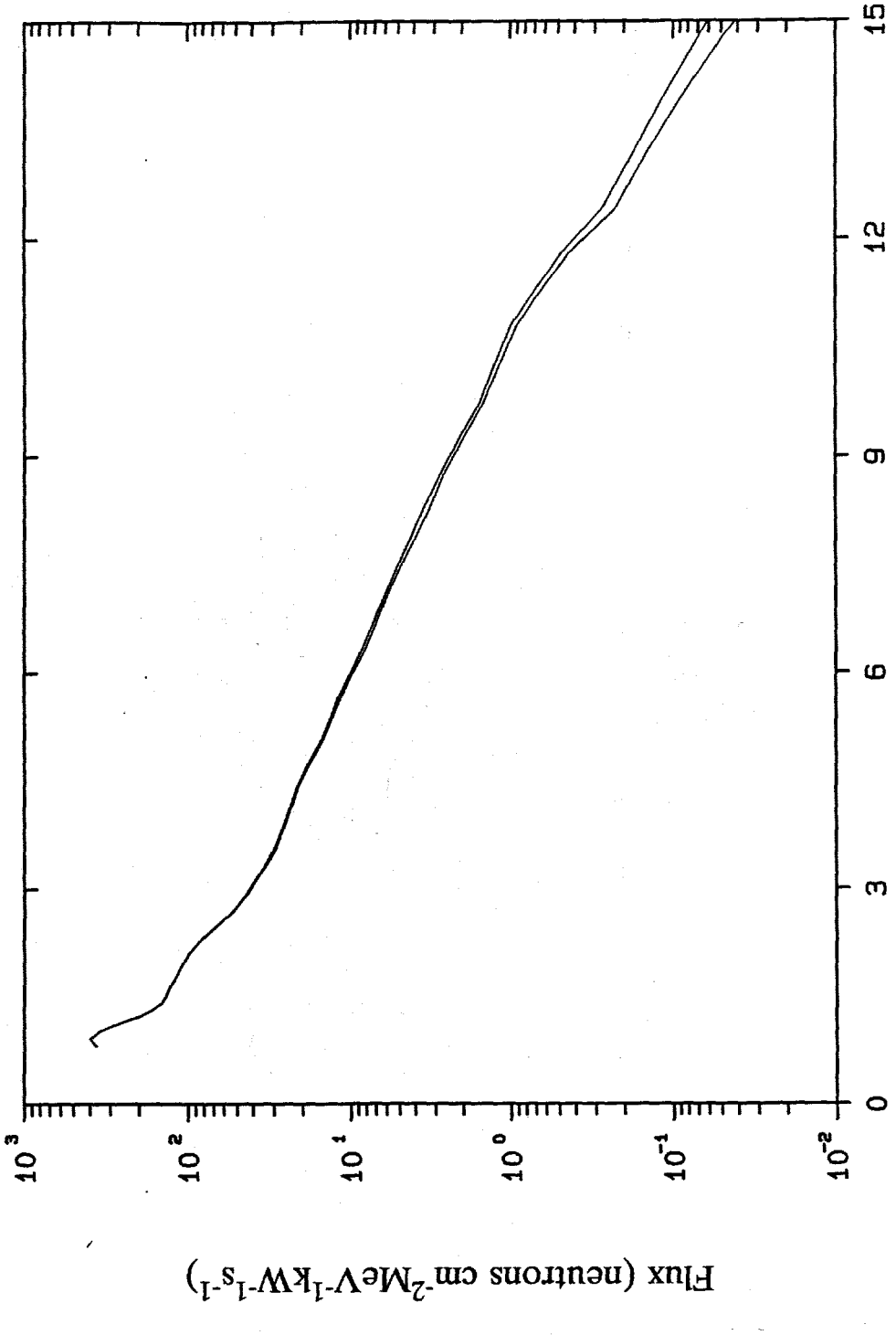

Figure 22. Spectrum of high-energy neutrons (>0.8 MeV) on centerline at 25 cm behind the lead slab (Item IIIA) Run 7939.

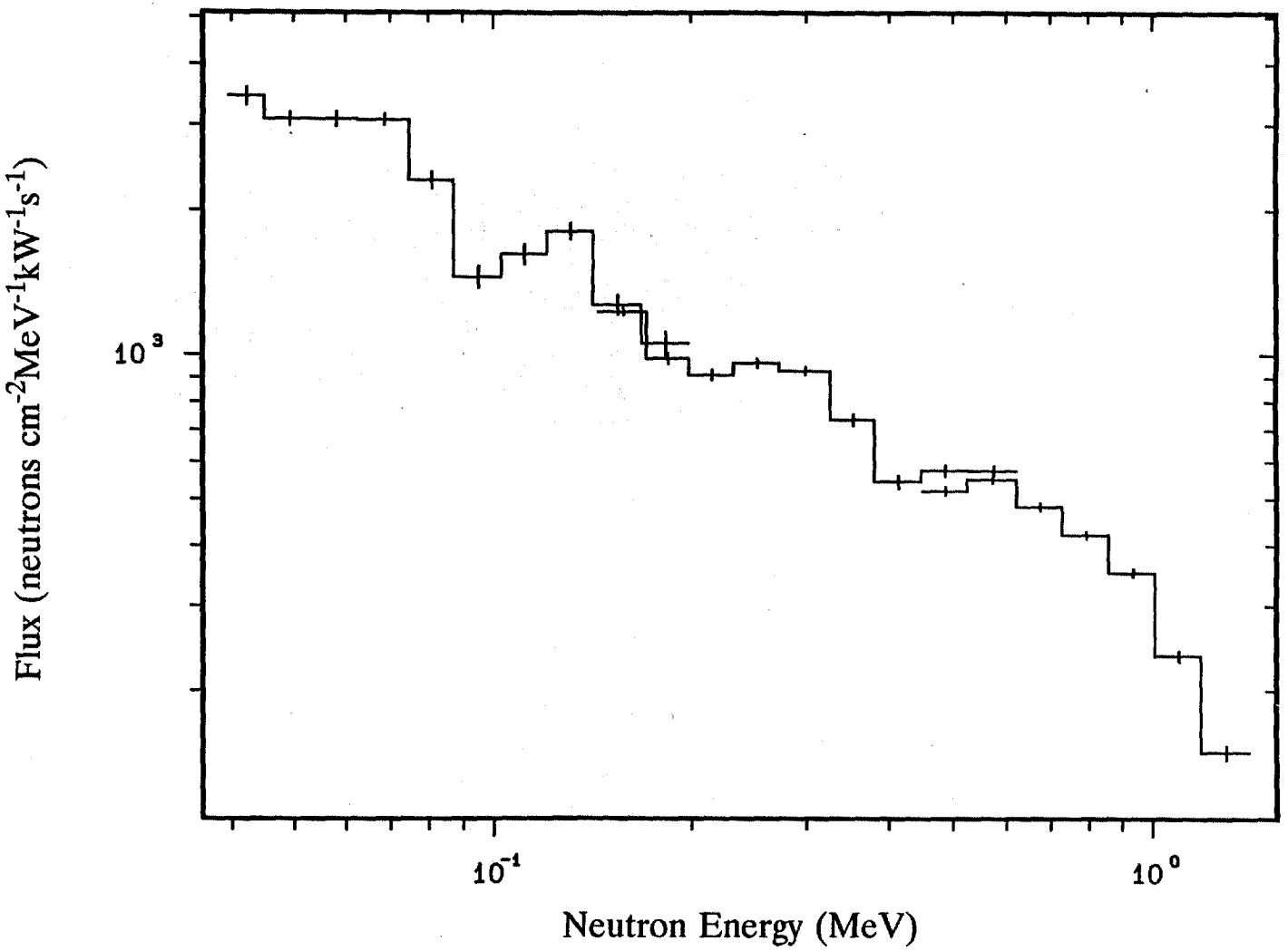

Figure 23. Neutron spectrum (50 keV to 1.4 MeV) on centerline at 25 cm behind the lead slab (Item IIIA) Runs 1609C, 1609B, 1609A.

ORNL/TM-12276
Distribution Category
UC-534

DISTRIBUTION

1. B. R. Appleton
2. J. A. Bucholz
3. L. B. Holland
4. F. J. Homan
5. H. T. Hunter
6-15. D. T. Ingersoll
16-17. F. J. Muckenthaler
18. J. V. Pace, III
19. J. A. Ray
20. C. O. Slater
21. R. R. Spencer
22. R. C. Ward
23. J. D. White
24. A. Zucker
25. Central Research Library
26-30. EPMD Reports Office
31. ORNL Y-12 Technical Library Document Reference Section
32-34. Laboratory Records
35. ORNL Patent Office

EXTERNAL DISTRIBUTION

36. Office of Assistant Manager for Energy Research and Development, DOE-OR, P.O. Box 2008, Oak Ridge, TN 37831-6269.

37. L. F. Blankner, Energy Research and Development, DOE-OR, P.O. Box 2008, Oak Ridge, TN 37831-6269.

38. Prof. Roger W. Brockett, Harvard University, Pierce Hall, 29 Oxford Street, Cambridge, Massachusetts 02138.

39. L. L. Carter, Westinghouse-Hanford Company, 400 Area Trailer 1, P.O. Box 1970, Richland WA 99352.

40. R. K. Disney, Westinghouse Electric Company, P.O. Box 158, Madison, PA 15663.

41. Prof. John J. Dorning, Department of Nuclear Engineering and Engineering Physics Reactor Facility, University of Virginia, Charlottesville, VA 22903.

42. P. B. Hemmig, Safety and Physics Branch, Office of Technology Support Programs, DOE-Washington, Washington, DC 20585.

43. Dr. James E. Leiss, Route 2, Box 142C, Broadway, VA 22815.

44. Prof. Neville Moray, Department of Mechanical and Industrial Engineering, 1206 West Green Street, Urbana, IL 61801.

45. Prof. Mary F. Wheeler, Department of Mathematical Sciences, Rice University, P.O. Box 1892, Houston, TX 77251.

46. K. Itoh, Power Reactor and Nuclear Fuel Development Corporation, Sankaido Building, 9-13, 1-Chome, Akasaka, Minato-Ku, Tokyo 107, Japan.

47. A. Shono, Oarai Engineering Center, Power Reactor and Nuclear Fuel Development Corporation, 4002, Marita, Oarai-Machi, Higashi-Kbaraki-Gun, Ibaraki-Ken, 311-13, Japan.

48. M. Tsutsumi, Power Reactor and Nuclear Fuel Development Corporation-Washington, Suite 715, 2600 Virginia Avenue NW, Washington, DC 20037.

49. K. Chatani, Power Reactor and Nuclear Fuel Development Corporation, 4002 Narita-Cho, O-Arai-Machi, Ibaraki-Ken, 311-13, Japan.

50-122. Given distribution as shown in DOE/OSTI-4500-R75, LMFBR-Physics: